Hydrogeochemical Evolution of Formation Waters Responsible for Sandstone Bleaching and Ore Mineralization in The Paradox Basin

Ji-Hyun Kim[1], Lydia Bailey[2], Chandler Noyes[1], Rebecca L. Tyne[3], Chris J. Ballentine[3], Mark Person[4], Lin Ma[5], Mark Barton[2], Isabel Barton[6], Peter W. Reiners[2], Grant Ferguson[1,7] and Jennifer McIntosh[1,7]

[1] Department of Hydrology and Atmospheric Sciences, The University of Arizona, Tucson, AZ, USA

[2] Department of Geosciences, The University of Arizona, Tucson, AZ, USA

[3] Department of Earth Sciences, University of Oxford, Oxford, England, UK

[4] Department of Earth and Environmental Science, New Mexico Tech, Socorro, NM, USA

[5] Department of Geological Sciences, University of Texas at El Paso, El Paso, TX, USA

[6] Department of Mining and Geological Engineering, The University of Arizona, Tucson, AZ, USA

[7] Department of Civil, Geological and Environmental Engineering, University of Saskatchewan, Saskatoon, Canada

ABSTRACT

The Paradox Basin in the Colorado Plateau has some of the most iconic records of paleofluid flow, including sandstone bleaching and ore mineralization, and hydrocarbon, CO_2 and He reservoirs, yet the sources of fluids responsible for these extensive fluid-rock reactions are highly debated. This study, for the first time, characterizes fluids within the basin to constrain the sources and emergent behavior of paleofluid flow resulting in the iconic rock records. Major ion and isotopic ($\delta^{18}O_{water}$; δD_{water}; $\delta^{18}O_{SO4}$; $\delta^{34}S_{SO4}$; $\delta^{34}S_{H2S}$; $^{87}Sr/^{86}Sr$) signatures of formation waters were used to evaluate the distribution and sources of fluids and water-rock interactions by comparison with the rock record. There are two sources of salinity in basinal fluids: 1) diagenetically altered highly evaporated paleo-seawater-derived brines associated with the Pennsylvanian Paradox Formation evaporites; and 2) dissolution of evaporites by topographically-driven meteoric circulation. Fresh to brackish groundwater in the shallow Cretaceous Burro Canyon Formation contains low Cu and high SO_4 concentrations and shows oxidation of sulfides by meteoric water, while U concentrations are higher than within other formation waters. Deeper brines in the Pennsylvanian Honaker Trail Formation were derived from evaporated paleo-seawater mixed with meteoric water that oxidized sulfides and dissolved gypsum and have high $^{87}Sr/^{86}Sr$ indicating interaction with radiogenic siliciclastic minerals. Upward migration of reduced (hydrocarbon- and H_2S-bearing) saline fluids from the Pennsylvanian Paradox Formation along faults likely bleached sandstones in shallower sediments and provided a reduced trap for later Cu and U deposition. The distribution of existing fluids in the Paradox Basin provides important constraints to understand the rock record over geological time.

INTRODUCTION

Multiple episodes of paleofluid flow through the Earth's crust are apparent in sedimentary basins worldwide (e.g., Bethke and Marshak, 1990; Hanor, 2001; Gupta et al., 2012; Engle et al., 2016). These episodes of fluid flow have resulted in widespread diagenesis (Hanshaw et al., 1971; Back et al., 1983; Machel, 1999), transport of hydrocarbons (Garven, 1989; Villegas et al., 1994), CO_2 and He (Crossey et al., 2009), and deposition of ore minerals (Cu, U, V, Co, Pb, Zn, etc; Kotzer and Kyser, 1995; Sanford, 1992; 1994). The Paradox Basin in the Colorado Plateau exhibits some of the most iconic examples/records of paleofluid flow, including extensive exposures of bleached (former red bed) sandstones, abundant hydrocarbon, CO_2 and He reservoirs and bitumen, widespread Cu and U-V mineralization, Fe/Mn oxide accumulations, and carbonate/silica metasomatism (e.g., M. Barton et al., 2018). We hypothesize that these multiple manifestations of paleofluid flow were the result of emergent behavior – defined as the result of spatial and temporal interactions of independent factors (e.g., pulsed migration and mixing of different fluid chemistries) leading to complex results that cannot be related to individual processes.

Previous studies in the Paradox Basin have shown that economic Cu deposits, hosted near faults in the siliciclastic Cretaceous Burro Canyon and Dakota formations, formed as a result of two separate fluid flow events (Hahn and Thorson, 2006; Thorson, 2018). Early migration of reduced, hydrocarbon-bearing saline fluids through fracture zones initially bleached the sandstones and reduced or removed the oxidized minerals (e.g., hematite reduction to pyrite or hematite dissolution and removal), enabling subsequent migration of oxidized Cu-bearing fluids to precipitate copper sulfide minerals at a reduced trap. However, the source of the reduced saline fluids and Cu is unclear.

Merin and Segal (1989) hypothesized that the early, reduced acidic fluids involved in bleaching of Jurassic sandstones were sourced from the geographically associated Mississippian petroleum reservoir in the Lisbon Valley oil field. Thorson (2018) inferred that the reduced saline fluids originated from

organic-rich shales (hydrocarbon source rocks) interbedded within evaporite units in the underlying Pennsylvanian Paradox Formation (Fm). Morrison and Parry (1986) suggested that the sources of Cu were immature red beds of the Permian Cutler Fm by analogy with prior work in other systems (Zielinski et al.,1983; Rose, 1989; Walker,1989; Rose and Bianchi-Mosquera, 1993). Alternatively, the moderately metals-enriched shales within the Paradox Fm could have provided adequate Cu (23 ppm average concentration; Tuttle et al., 1996), if an appropriate transporting fluid were available and the geochemical and hydrologic conditions were permissive (Thorson, 2018).

Genetic models for U and V deposits in the Jurassic Morrison and Triassic Chinle formations in the northeastern Paradox Basin have also invoked mixing of two different fluids – dilute, oxidized, U- and V-bearing groundwaters (local flow system) and reduced saline fluids carrying hydrocarbons, humate, or other reduced species derived from organic matter (regional flow system) – at density-stabilized interfaces (Turner-Peterson et al., 1986; Northrop et al., 1990; Sanford, 1994). Similar to the Cu deposits, U and V deposits are found in sandstones that were previously bleached and commonly contain remnant hydrocarbons (Shawe, 2011; I. Barton et al., 2018). The question remains whether reduced and oxidized fluids were sequential or coeval to U and V mineralization in reduced traps. The source of U is debated given the lack of direct evidence connecting deposits to potential uraniferous source rocks, which include tuffaceous volcanic material in Morrison and Chinle formations (Waters et al., 1949; Christiansen et al., 2015); granitic debris (Thorson, 2018); or Paradox Fm organic-rich shales (which contain up to 70 ppm U, Whidden et al., 2014, Thorson, 2018). Similarly, the source of V has yet to be identified.

The Paradox Basin also hosts stratigraphically and structurally-controlled Fe/Mn oxides and carbonates (e.g., from hollow hematite pipes to large nodules to massive veins) at the top of the Navajo and Entrada sandstones (Chan et al., 2000; Garcia et al., 2018). These may have been deposited by saline fluids thought to have been reduced via interaction with organic acids, H_2S, petroleum or CO_2 reservoirs (Chan et al., 2000; Loope et al., 2010; Wigley et al, 2012). The deeper reducing fluids are interpreted to

have removed Fe and Mn in red bed sandstones and locally precipitated Fe/Mn oxides under more oxidizing conditions by mixing with oxidized groundwater (Chan et al., 2000; Reiners et al., 2014; I. Barton et al., 2018; Garcia et al., 2018), which could have also contributed to the supergene alteration and oxidation of Jurassic U-V ore deposits (Shawe, 2011). However, without adequate geochemical and isotopic data on formation waters it is difficult to verify the source and pathways of fluids responsible for widespread sandstone bleaching and metallic (Cu, V, U, Fe and Mn) mineralization.

Waters of variable salinities remain in the Paradox Basin today – from shallow fresh to brackish aquifers to surficial brine seeps and deep, saline formation waters. The few studies of existing fluids in the Paradox Basin lack key chemical (e.g., Br, Cu, and U) and isotopic (e.g., $\delta^{18}O/\delta D$) data (Hanshaw and Hill, 1969; Thackston et al., 1981; Williams-Stroud, 1994), necessary to delineate sources of salinity and metals, and proportions of fluid mixing. Previous investigations of paleofluid flow and solute transport have been primarily focused on the rock record with inferences about the origin, composition, flowpaths and mixing of paleofluids (Shawe, 1968; Morrison and Parry, 1986; Breit et al., 1990; Chan et al., 2000; Loope et al., 2010; Wigley et al., 2012). This study provides, for the first time, a detailed investigation of the chemical and isotopic composition, distribution, and mixing of various fluids in different formations within the Paradox Basin and compares them to the rock record, to reveal key chemical and hydrogeologic processes and their timing to demonstrate emergent behaviors in sedimentary basin systems.

STUDY AREA

The Paradox Basin covers ~85,000 km^2 of southeastern Utah and southwestern Colorado on the Colorado Plateau (Fig. 1a). The basin developed as a northeastward-deepening flexural response to crustal loading by reverse faulting that generated the Late Paleozoic Uncompahgre uplift of the ancestral Rocky Mountains (Baars and Stevenson, 1982; Barbeau, 2003; Leary et al., 2017). The subsidence of northeastern side of the Paradox Basin led to initial deposition of carbonates, shales and siltstones,

106 followed by deposition of up to 2.5 km of marine evaporites in the Pennsylvanian Paradox Fm (Hite et al.,
107 1984; Nuccio and Condon, 1996). Arkosic sandstone of the Cutler Fm and related units sourced from the
108 Uncompahgre Uplift overlie the Paradox Fm and underlie the Triassic through Cretaceous eolian and
109 fluvial sediments (Fig. 1c). Beginning in the Permian, plastic flow of the Paradox evaporites created salt
110 anticlines, associated faults, and sub-basins, such as in the Lisbon and Paradox Valley areas, along the
111 northeastern side of the basin (Fig. 1a).

112 **Geological Background**

113 Above the Proterozoic crystalline basement, basal Cambrian formations consist of conglomerate
114 – mixtures of sandstone, limestone, and shale, limestone, and dolomite deposited in diverse marine
115 conditions – in the Paradox Basin (Nuccio and Condon, 1996). Ordovician, Silurian, and Early and
116 Middle Devonian age formations are not found in the Paradox Basin because of post-Cambrian erosion
117 (Nuccio and Condon, 1996). The Late Devonian Elbert Fm (Fig. 1c and 2) was deposited in a shallow
118 marine environment and is composed of the basal McCracken Sandstone (Ss) member and a dolomite and
119 shale upper member (McBride, 2016). Sea-level fall after deposition of the Ouray Limestone (Ls) ended
120 the Devonian Period (Fig. 1c and 2). Renewed transgression of the sea from the west initiated deposition
121 of the Mississippian Leadville Ls or Redwall Ls (Fig. 1c and 2) with a series of transgressive and
122 regressive events (Nuccio and Condon, 1996). A final regression of the sea in the Late Mississippian
123 exposed the limestones to a subaerial environment. A regolith developed on this surface, as well as
124 cavities and karst topography formed by fresh water in some exposed areas (Sanford, 1990a; 1990b;
125 Nuccio and Condon, 1996). A large northwest-trending graben-faulted anticline consisting of late
126 Precambrian through Mississippian rocks is thought to have provided the site of Pre-Pennsylvanian
127 reservoir facies and thick Pennsylvanian salt deposition (Fig. 1b) (Baars ,1966).

128 The Paradox Fm, an extensive evaporitic unit (up to 1.8 km thick where the salt is not severely
129 disturbed), consisting of cyclical dolomite, black shale, anhydrite, halite, sylvite, carnallite and other

bittern facies salts, that represent repeated marine flooding of the basin and evaporation in an arid climate (Fig. 1 and 2) (Hite and Lohman, 1973; Hite and Buckner, 1981; Nuccio and Condon, 1996). Interbedded, black dolomitic shales, especially the Ismay-Desert Creek and Cane Creek members of the Middle Pennsylvanian Paradox Fm (Fig. 2), contain up to 11 % total organic carbon, which are an important source of hydrocarbons (Nuccio and Condon, 1996), and are moderately metal-rich (Tuttle et al., 1996; Whidden et al. 2014). In the northeastern part of basin, the relatively thick Tertiary sedimentary sequence combined with increased basinal temperatures in the Tertiary resulted in high thermal maturities (0.1 to 0.5 of production index (PI) for the Ismay-Desert Creek members; >0.5 of PI for the Cane Creek member) compared to the south-central to southwestern part of basin (<0.1 of PI for the Ismay-Desert Creek members; >0.1 of PI for the Cane Creek member; Nuccio and Condon, 1996). In the Lisbon Valley, in the structurally deeper part of the basin, significant oil generation began around 79 Ma for the Ismay-Desert Creek members and 100 Ma for the Cane Creek member – much earlier than other oil fields in the basin – and the source rocks reached their maximum burial around 25 Ma (Nuccio and Condon, 1996). In the southwestern part of the basin (e.g., Greater Aneth oil field), the Paradox Fm is dominated by shelf carbonates, including algal-mound buildups that act as petroleum reservoirs (Fig. 1b).

The overlying Pennsylvanian Honaker Trail Fm (Fig. 1c and 2) consists of limestone, sandstone, and shale deposited in a cyclic pattern from the evaporitic marine conditions of the Paradox Fm to normal marine conditions. The Honaker Trail Fm contains significant eolian and fluvial beds, especially on the northeastern side of the basin (Nuccio and Condon, 1996). The Permian Cutler Fm (Fig. 1c and 2) is mostly a product of erosion of the Uncompahgre Uplift and consists of arkosic sandstone (Cater and Craig, 1970; Nuccio and Condon, 1996). Deposition of the Cutler Fm was strongly influenced by the concurrent growth of the salt walls with consequent impact on facies distribution and, ultimately, hydrologic characteristics (Trudgill, 2011; Lawton et al., 2015).

153 Triassic and Jurassic sedimentation in the Paradox Basin was influenced by intrusion of laccoliths
154 (28 ± 1 Ma; Nuccio and Condon, 1996; Friedman and Huffman, 1997; M. Barton et al., 2018; Murray et
155 al., 2019), such as the La Sal, Abajo, and Ute mountains (Fig. 1a). Large volumes of volcanic ash were
156 deposited in the Triassic and Jurassic sediments derived from the Mesozoic magmatic arc (Christensen et
157 al., 1994). During the denudation of the Colorado Plateau in the Late Tertiary to Holocene (<10 Ma:
158 Lazear et al., 2011; <4-6 Ma: Murray et al., 2016; Murray et al., 2019), most of the Cretaceous (and
159 Cenozoic) rocks of the Paradox Basin, for example, the Mancos Shale, were removed by erosion (Nuccio
160 and Condon, 1996). Emplacement of the laccoliths and recent denudation of the Colorado Plateau also
161 created higher topographic gradients.

162 The Triassic Moenkopi and Chinle formations are composed of siltstone, shale, conglomerate,
163 and sandstones and host U and V deposits in the Slick Rock district (Fig. 2; Shawe, 2011; I. Barton et al.,
164 2018). The Jurassic formations are composed of eolian sandstones and fluvio-lacustrine sandstones and
165 shales (Fig. 2). The Jurassic Wingate Ss, Navajo Ss and Entrada Ss include bleached/red bed sandstones
166 (Fig. 2). The lower Salt Wash member of Jurassic Morrison Fm contains bleached sandstones, which host
167 economic U and V deposits in the Slick Rock district and Lisbon Valley (Shawe, 2011; I. Barton et al.,
168 2018), as well as Cu deposits in the Lisbon Valley (Fig.2; I. Barton et al., 2018). The upper Brushy Basin
169 member of Jurassic Morrison Fm is dominated by mudstone, siltstone, and volcanic ash, which is
170 considered as the source for U (Fig. 2). The early Cretaceous age Burro Canyon Fm, overlying the
171 Jurassic Morrison Fm, is composed of conglomeratic sandstone and mudstone derived from fluvial and
172 flood plain deposits (Nuccio and Condon, 1996) and hosts economic Cu deposits in bleached zones in the
173 Lisbon Valley (Fig.2; Thorson, 2018). The overlying Dakota Ss also contains economic Cu deposits in
174 the Lisbon Valley (Fig. 2; Thorson, 2018). All of the known Cu deposits in the Lisbon Valley lie along
175 the Lisbon Valley Fault system.

176 The salt anticlines and associated faults evolved along on the northeastern portion of the basin,
177 for example in the Paradox and Lisbon valleys (Fig. 1c; Chan et al., 2000), as Permian through Jurassic
178 sediments eroded from Uncompahgre Uplift were deposited onto thick sequences of the Middle
179 Pennsylvanian Paradox Fm evaporites (Fig. 1a; Nuccio and Condon, 1996). Significant fault systems
180 started to grow in the Permian (Doelling, 1988; Trudgill, 2011) and continued through the Mesozoic (e.g.,
181 Hartley and Evenstar, 2018) and into the Cenozoic (Cater and Craig, 1970; Lawton and Buck, 2006) with
182 collapse due to salt withdrawal and/or dissolution. In some of the salt anticlines, for example the Paradox
183 Valley anticline, the bounding faults extend below the anticline to cut Pre-Pennsylvanian rocks (Fig. 1c,
184 Baars, 1966; Hite and Lohman, 1973).

185 **Hydrological Background**

186 Regional groundwater flow in the Paradox Basin is generally towards the southwest from major
187 recharge areas along the Uncompahgre Uplift and San Juan Mountains towards the Colorado River
188 (Hanshaw and Hill, 1969). Deviations from regional-scale flow occur due to barriers to flow, such as
189 dikes and faults or the influence of intrabasin recharge areas (e.g., topographic highs created by laccolith
190 intrusions; Hanshaw and Hill, 1969; Thackston et al., 1981). In the upper hydrostratigraphic unit,
191 consisting of the post-Paleozoic and Permian formations and the Upper Honaker Trail Fm above the salt
192 (Fig. 1c), groundwater flow is mainly controlled by topography (Hanshaw and Hill, 1969; Thackston et
193 al., 1981; King et al., 2014). The presence of salt anticlines and topographically-driven groundwater
194 recharge within the basin are responsible for the discharge of highly saline water into surface water in the
195 valleys in the northeastern region (King et a., 2014). For example, meteoric waters recharged from the La
196 Sal Mountains flow downgradient into sediments beneath the Paradox Valley, dissolve evaporites in the
197 underlying salt anticline of the Paradox Fm, and discharge as brines into the Dolores River with an
198 average total dissolved solids (TDS) concentration of 260 g/L, prior to installation of brine pumping wells
199 (Chafin, 2003; King et al., 2014). A similar flow system has been evoked for solute transport in the

Gypsum Valley (Reitman et al., 2014) and the La Sal Mountains provide recharge to the Glen Canyon Group in the Spanish Valley with discharge to the Colorado River (Gardner et al., 2020). We hypothesize recharge from the La Sal Mountains drives salt dissolution and saline water discharge into Salt Creek in the Sinbad Valley.

The middle hydrostratigraphic unit, composed of the lower Honaker Trail and Paradox Salt formations (Fig. 1c), is a regional confining unit (Thackston et al., 1981; Hanshaw and Hill, 1969). Regional Honaker Trail Fm permeabilities range between 6×10^{-17} and 5×10^{-14} m^2 (Woodward-Clyde Consultants, 1982). Permeabilities reported for the isolated, most porous zone within the Paradox Fm by the oil industry range between 1×10^{-16} and 5×10^{-13} m^2 (Woodward-Clyde Consultants, 1982). While no direct measurements of evaporite permeability are available for the Paradox Fm, they are likely very low (Beauheim et al. 1993).

The Mississippian Leadville Ls through Devonian Elbert Fm are considered as a single, lower hydrostratigraphic unit beneath the salt (Fig. 1c) with a regionally extensive flow system toward the southwest (Hanshaw and Hill, 1969; Thackston et al., 1981; Woodward-Clyde Consultants, 1983). This unit receives recharge locally around groundwater mounds in the Abajo and La Sal mountains or along the margins of the salt anticlines (Hanshaw and Hill, 1969; Thackston et al., 1981). The lower potentiometric surface of the lower hydrostratigraphic unit compared to the upper hydrostratigraphic unit has been interpreted to suggest that fluids today flow downward throughout the Paradox Basin, although this lower aquifer system is less affected by local topography than the upper aquifer system (Hanshaw and Hill, 1969). Regional lower unit permeabilities vary between 2×10^{-17} and 2×10^{-12} m^2 for the Leadville Ls and between 2×10^{-16} and 9×10^{-14} m^2 for Devonian rocks (Woodward-Clyde Consultants, 1982). Precambrian rocks, underlying the Paradox Basin have up to > 9 % porosity and several open and hairline fractures (Bremkamp and Harr, 1988), indicating there is likely flow within the basement rocks, although there is little hydrologic data (e.g., permeability values). Measured crystalline basement permeability

from hydraulic tests elsewhere have reported relatively high permeability values (10^{-15} m^2; Stober and Bucher, 2007), but there is significant variability (Achtziger-Zupančič et al., 2017). Induced seismicity reported by Ake et al. (2005) indicated that the fluid pressure associated with brine injection into the Leadville Ls along the Dolores River propagated downward more than 1 km into the underlying crystalline basement suggesting at least moderate permeability conditions.

METHODS

Sample Locations

To constrain the composition, origin and mixing relationships of different fluid types in the Paradox Basin present today, a total of 44 water samples were collected from various depths (0-2 km) in 2018 and 2020 (Table 1). Water samples were collected from local rivers, seeps, shallow groundwater monitoring wells, shallow brine extraction wells, deeper oil and gas wells, and one deep lithium exploration well where access was permitted. The approximate spatial location and geologic formation of water samples are shown in Figs. 1a and 2. The formation water sample from the lithium exploration well (northwest of Moab, Utah) is from the Cane Creek member of the Pennsylvanian Paradox Fm. Eleven formation water samples were collected from oil and gas wells in the Pennsylvanian Honaker Trail, Mississippian Leadville, and Devonian McCracken formations in the Lisbon Valley near the Utah-Colorado border. Six groundwater samples were also collected from monitoring wells in the Lisbon Valley completed in the Jurassic Navajo and Cretaceous Burro Canyon formations. In the Paradox Valley, in western Colorado, four surface water samples were collected from the Dolores River and four groundwater samples were collected from the U.S. Bureau of Reclamation's brine pumping wells completed in the Dolores River alluvial aquifer. In the Sinbad Valley, in western Colorado, three surface water samples were collected from Salt Creek and two groundwater samples from seeps adjacent to the creek. In the Greater Aneth oil field, south of Blanding, Utah, 13 formation water samples were collected

from oil wells producing from the Ismay-Desert Creek members of Pennsylvanian Paradox Fm. Formation water samples from the Greater Aneth oil field were taken from areas with historical water flooding activity (identified by asterisk symbol in Table 1).

Sample Collection

In the oil and gas fields, a mixture of oil and produced water was collected directly from the well head (where possible) or from the oil-brine separator tank (when oil to water cuts were high) into a 19 L Nalgene carboy filled to the top and capped, following similar procedures as Kharaka et al. (1987) and McIntosh et al. (2002). After the formation water had settled to the bottom of the carboys (with oil on top), the formation water was removed through a spigot at the bottom of the carboy and filtered through a 1.6 μm glass fiber filter to remove any residual oil. For samples from the lithium exploration well, groundwater monitoring wells, and brine pumping wells, water was collected from the well head. Water samples from the flowing Dolores River and Salt Creek, and seeps along Salt Creek were collected using syringes.

All water samples were filtered through 0.45 μm nylon membrane filters into pre-cleaned HDPE bottles. Sample aliquots for cations, trace metals and $^{87}Sr/^{86}Sr$ were acidified by adding two drops of concentrated Optima-grade nitric acid into 30 mL pre-acid-washed HDPE sample bottles. All samples were kept on ice in the field and at ~4 ^{o}C in the refrigerator in the laboratory prior to analysis. pH, specific conductance and temperature were measured using a Thermo Scientific Orion 5 Star meter and electrodes in the field. Both pH and specific conductance meters/electrodes were calibrated daily before each sampling event. Alkalinity was measured within 12 hours by gran titration (Gieskes and Rogers, 1973) and density was measured using a Mettler Toledo hand-held density meter.

Analyses

All water samples were analyzed for cations, anions, trace metals, $\delta^{18}O$ and δD of water, $\delta^{34}S$ and $\delta^{18}O$ of SO_4 and $^{87}Sr/^{86}Sr$. Select water samples were analyzed for aqueous H_2S concentrations and $\delta^{34}S$ of H_2S. Cation (Ca, Mg, Na, and K) and Si concentrations of all samples prior to 2020 were analyzed via Inductively Coupled Plasma-Optical Emission Spectrometry (ICP-OES, Perkin-Elmer 5300DV) in the Department of Hydrology and Atmospheric Sciences at the University of Arizona (UA). Analytical precision (1σ) was <5 % for all cations using a standard reference sample (USGS T219). Anions (Cl, Br, and SO_4) were measured via Ion Chromatography (DIONEX ICS-3000) with an IonPac AS23 column in HAS at UA. Analytical prevision (1σ) was <0.8 % errors for all anions using a standard reference sample (USGS M126). Trace metals were determined via ICP-Mass Spectrometry in the Department of Geological Sciences at the University of Texas at El Paso (UTEP) in the range of 3 % to 24 % analytical precision (1σ) using a standard reference sample (USGS T217). Charge balances were <5 % for all water samples. All water samples collected in 2020 were analyzed for cations and anions in the Environmental Analytical Laboratories at the Saskatchewan Research Council. For the additional samples, Ca, K, Na and SO_4 were determined using an ICP-OES. Br was analyzed by an ICP-MS. Cl was determined via automated colorimetric determination on a ThermoFisher Gallery Plus Discrete Analyzer. Aqueous H_2S was fixed in the field by reacting with pre-weighed $CdCl_2$. Precipitated CdS was isolated from water, dried and weighed to determine the H_2S concentration. Because aqueous H_2S can be degassed during sampling, the calculated H_2S concentration is the minimum H_2S concentration in water sample.

$\delta^{18}O$ and δD of water was measured by laser spectrometer (Los Gatos Research DLT-100 Liquid Water Isotope Analyzer) in HAS at UA. Analytical precision (1σ) for all samples was 0.1 ‰ for $\delta^{18}O$ and 0.5 ‰ for δD. Fourteen duplicate brine samples of relatively high TDS (>200 g/L) were also analyzed for $\delta^{18}O$ and δD via isotope ratio mass spectrometer (Finnigan Delta S) in the Environmental Isotope Laboratory (EIL) in the Geosciences Department at UA. Corresponding $\delta^{18}O$ and δD data from the mass spectrometer were converted from an activity basis to a concentration basis using the empirical methods of Sofer and Gat (1972; 1975). $^{87}Sr/^{86}Sr$ were determined using a Nu Plasma multiple collector-

Inductively Coupled Plasma-Mass Spectrometer at UTEP. Analytical precision of strontium isotopic ratios was 0.00009 for all samples. $\delta^{34}S_{SO4}$, $\delta^{18}O_{SO4}$, and $\delta^{34}S_{H2S}$ were measured by continuous-flow gas-ratio mass spectrometer (ThermoQuest Finnigan Delta PlusXL and Thermo Electron Delta V, respectively) in the EIL at UA. Analytical precision for $\delta^{34}S_{SO4}$ and $\delta^{18}O_{SO4}$ was 0.2 ‰ and 0.4 ‰, respectively. New results from this study were supplemented with the limited existing hydrochemical data for the Paradox Basin (Mayhew and Heylmun, 1965; Nuckolls and McCulley,1987; Rosenbauer et al., 1992; Spangler et al., 1996; Naftz et al., 1997; Kharaka et al., 1997; Blondes et al., 2018).

PHREEQC modeling

The PHREEQC code (version 3.6.2) was used to calculate saturation indices of barite, calcite, dolomite, gypsum, halite, sylvite, CuS, chalcocite, and chalcopyrite, using analyzed chemical data, including pH, alkalinity, Ba, Br, SO_4, Ca, Mg, Na, K, Sr, H_2S, Mn, Fe, Cu, and U. The concentrations of HCO_3 and H_2CO_3 were calculated with PHREEQC using the same chemical dataset to compute dissolved inorganic carbon (DIC) values; CO_3 concentrations were too low to consider. The Pitzer database based on Pitzer equations (Plummer, 1988) was used to calculate ion activity coefficients for the high ionic strength brackish water and brine samples. The Pitzer database was modified to include species (e.g., Mn, Fe, Cu, and U) from the PHREEQC database, which were not included in the original Pitzer database.

In order to simulate mixing proportions of various water sources contributing to groundwater collected from the brine pumping wells and formation water collected from the Mississippian Leadville Ls, we performed inverse mixing modeling (ST1 and 2; Appelo and Postma, 2004) using the Pitzer database. Inverse mixing modeling assumes that the mole-balance of selected elements for a final solution is evolved from a mixture of two initial solutions. For the fresh, meteoric water endmember as a first initial solution, the average concentrations of major ions (Ca, Na, K, Cl, Br, HCO_3, and SO_4) and pH of shallow groundwaters in the Burro Canyon Fm and Navajo Ss were used. The major ions and pH of formation water in the Cane Creek member of the Paradox Fm were used as the second initial solution,

representing the most evaporated paleo-seawater endmember. A final solution for each inverse mixing model used the average concentrations of major ions and pH of groundwater from the brine pumping wells or formation water collected from the Leadville Ls. Halite, gypsum, anhydrite, sylvite and calcite were defined as dissolution phases to simulate dissolution of evaporites. Mole-balance equations for all elements that were found in the phases input (e.g., Na, Ca, Cl, SO_4, K, and HCO_3) were automatically included in inverse modeling with the default uncertainty limits to determine the mixing proportions under the specific dissolution phases. Br was also considered as a balance element, which was essential to determine the proportions of the second (evaporated paleo-seawater) endmember in each final solution.

RESULTS

Chemical and isotopic compositions of all water samples are summarized in Table 2. The TDS of groundwater in the Cretaceous Burro Canyon Fm and Jurassic Navajo Ss is 0.5 to 2.0 g/L, within the range of fresh to brackish water (Stanton et al., 2017). Dolores River and Salt Creek samples show a wide range of TDS (0.5 to 16.5 g/L and 1 to 87 g/L, respectively) from freshwater to brine. Groundwater samples from shallow brine pumping wells in the Paradox Valley, overlying a salt anticline structure, have high TDS (245 to 256 g/L), hereinafter referred to as the "salt anticline brine." Most of the formation water samples from the Pennsylvanian Honaker Trail Fm, Mississippian Leadville Ls, and Devonian McCracken Ss are considered brines with 70 to 308 g/L TDS. Formation water samples from the Ismay-Desert Creek members of Pennsylvanian Paradox Fm in the Greater Aneth oil field are also considered brines (hereafter the "Desert Creek brine") with 63 to 255 g/L TDS, with the exception of one sample (Anasazi 1) which has 34 g/L TDS (close to seawater salinity). The highest TDS (335 g/L) formation water sample is from the Cane Creek member of the Paradox Fm (hereafter the "Cane Creek brine").

Based on experimental data on evaporated modern seawater by McCaffrey et al. (1987), the enrichment or depletion of major cations in basinal brine samples were plotted relative to Br concentration to determine the origin of salinity and chemical modifications via diagenetic reactions (Fig.

342 3). Most of the deep basinal brine samples, except for formation waters from the Leadville Ls, are
343 depleted in Na, K and Mg and enriched in Ca relative to evaporated seawater. In contrast, the salt
344 anticline brine and brines from the Leadville Ls are enriched in Na, K and Ca and depleted in Mg relative
345 to evaporated seawater. The majority of brine samples from the Paradox Basin have relatively low
346 measured alkalinity (< 7.97 meq/L) and pH (5.18-6.75) values (Table 1) compared to endogenic springs
347 in the Grand Canyon region of the Colorado Plateau, which have higher alkalinity values (up to 37.70
348 meq/L, assuming HCO_3 is dominant) and slightly acid to neutral pH (6-7.5) (Crossey et al., 2006). Three
349 brine samples (TOHO 1, McIntyre 17-21, and Lisbon B8-10) have elevated alkalinity (11.36-12.55
350 meq/L) and pH (6.78-7.25) values. Five samples of Desert Creek brines and one of the Honaker Trail Fm
351 brines exhibit elevated DIC values (21.48-42.57 meq/L) with high H_2CO_3 concentrations, calculated using
352 PHREEQC, relative to other brines (Table 3).

353 The salt anticline brine, salt anticline-related surface water and brines from the Leadville Ls have
354 higher Cl/Br and Na/Br than modern seawater (Riley and Chester, 1971; Fig. 4a) and fall on the halite
355 dissolution line with a 1:1 relationship between Na and Cl (Hanor, 2001; Grasby and Chen, 2005; Gupta
356 et al., 2012; Engle et al., 2016). The salt anticline brine, which plots on the halite saturation line in Fig. 4b
357 (Grasby and Chen, 2005), is at saturation with respect to halite and gypsum, and is undersaturated with
358 respect to sylvite (Table 3). The Leadville Ls brine is at saturation with respect to gypsum and is
359 undersaturated with respect to halite and sylvite (Table 3). In contrast, brines in the Honaker Trail,
360 Paradox (Desert Creek and Cane Creek members), and McCracken formations exhibit lower Cl/Br and
361 Na/Br than seawater (Fig. 4a) and plot along or to the right of the evaporated modern seawater line
362 (McCaffrey et al., 1987; Fig. 4b). The Cane Creek brine has the lowest Cl/Br and Na/Br, and highest Cl
363 (6,083 mmol/L) and Br (38.91 mmol/L) concentrations compared to other basinal brines in this study.

364 Inverse modeling using major ion chemistry was conducted to quantify the various sources of
365 salinity and mixing of different fluids. Note that for inverse mixing modeling for the salt anticline brine,

366 we assumed that some portion of evaporated paleo-seawater within the Paradox Fm shale interbeds
367 (represented by the Cane Creek brine chemical composition) may have mixed with brines formed by
368 dissolution of the Paradox Fm evaporites in the salt anticline. There were two possible modeling results
369 for the salt anticline brine, both indicating mixing of 97.5 % meteoric water and 2.4 % Cane Creek brine,
370 accompanied by dissolution of 4.1 ± 1.6 moles of halite, 0.04 ± 0.001 moles of gypsum (or anhydrite) and
371 0.1 ± 0.05 moles of sylvite. For the inverse mixing modeling for brines in the Mississippian Leadville Ls,
372 we assumed that evaporated paleo-seawater within the Paradox Fm shale interbeds (represented by the
373 Cane Creek brine) could have migrated via diffusion (Hanor and McIntosh, 2007) into underlying
374 Mississippian formations. There were four possible modeling results for Leadville Ls brine, showing
375 mixing of 95.8 % meteoric water and 4.2 % Cane Creek brine, accompanied by the dissolution of 0.9 ±
376 0.1 moles of halite, 0.005 ± 0.0001 moles of calcite, 0.01± 0.002 mole of gypsum (or anhydrite) and 0 to
377 0.02 moles of sylvite.

378 $\delta^{18}O_{water}$ and δD_{water} values were used to constrain the source of water and mixing relationships of
379 different fluids (Table 4 and Fig. 5), plotted with the local meteoric water line (LMWL; Kendall and
380 Coplen, 2001) and the global meteoric water line (GMWL; Craig, 1961). $\delta^{18}O_{water}$ and δD_{water} values for
381 the salt anticline brine, salt anticline-related surface waters, and groundwater in the Burro Canyon Fm and
382 Navajo Ss plot closest to the LMWL. Some of the groundwater samples of the Burro Canyon Fm are
383 within the range of local modern precipitation in the Abajo Mountains, which ranges from -16.7 to -15.8
384 ‰ $\delta^{18}O_{water}$ and -122 to -115 ‰ δD_{water} (Spangler et al., 1996). The four salt anticline brine samples have
385 consistent $\delta^{18}O_{water}$ (-14.71 to -14.65 ‰) and δD_{water} (-110.86 to -110.18 ‰) values. The Salt Creek
386 surface waters have lower $\delta^{18}O_{water}$ (-14.71 to -12.29 ‰) and δD_{water} (-108.81 to -97.77 ‰) values, while
387 the Dolores River has relatively high $\delta^{18}O_{water}$ (-13.30 to -8.75 ‰) and δD_{water} (-94.00 to -73.02 ‰) values.
388 Most of the brines from the Honaker Trail, Paradox, Leadville, and McCracken formations plot to the
389 right of the LMWL and are consistent with $\delta^{18}O_{water}$ and δD_{water} values of fluid inclusions in halite in the
390 Paradox Fm (Petrychenko et al., 2012). The Cane Creek brine sample plots furthest to the right of the

LMWL with the highest $\delta^{18}O_{water}$ (4.98 ‰) and δD_{water} (-7.57 ‰) values. The Honaker Trail Fm brines show a linear mixing trend in stable water isotope values between an evaporated endmember and the LMWL, which has a different slope than the linear mixing trend for Desert Creek brines (Fig. 5).

$\delta^{34}S_{SO4}$ and $\delta^{18}O_{SO4}$ values were examined to identify the sources of SO_4 (Table 4 and Fig. 6). $\delta^{34}S_{SO4}$ and $\delta^{18}O_{SO4}$ values of groundwater from the Burro Canyon Fm and Navajo Ss plot in the established fields of sulfide oxidation and soil (Clark and Fritz, 1997; Fig. 6a). Groundwater in the Burro Canyon Fm has relatively high SO_4 concentrations (up to 10.3 mmol/L) in contrast to the Navajo Ss (up to 1.5 mmol/L SO_4; Fig. 6b). $\delta^{34}S_{SO4}$ and $\delta^{18}O_{SO4}$ values of the salt anticline brine, the Salt Creek and brines from the Paradox, Leadville, and McCracken formations plot in the established field of evaporites (Fig. 6a). $\delta^{34}S_{SO4}$ and $\delta^{18}O_{SO4}$ values of the Cane Creek brine correspond to previously reported values for Paradox Fm evaporites (Holt et al., 2014; Chen et al., 2016). The salt anticline brine and Salt Creek have high SO_4 concentrations (65.8-82.7 mmol/L and 21.5-31.7 mmol/L, respectively) compared to brines from Honaker Trail, Paradox, Leadville, and McCracken formations (up to 15.4 mmol/L; Fig. 6b). $\delta^{34}S_{H2S}$ values were only measured for select salt anticline brine and Salt Creek samples (Table 4) and $\varepsilon^{34}S_{SO4\text{-}H2S}$ values of these waters are 24-39 ‰ within the range of bacterial sulfate reduction (Clark and Fritz, 1997). $\delta^{34}S_{SO4}$ values of the Honaker Trail Fm brines vary between the sulfide oxidation and evaporite fields despite consistent SO_4 concentrations (Fig. 6b). Dolores River waters and Honaker Trail Fm brines each show a linear mixing trend between SO_4 sourced from sulfide oxidation and evaporites (Fig. 6a). There is no negative correlation between $\delta^{34}S_{SO4}$ values and SO_4 concentrations for the Dolores River or Honaker Trail water samples (Fig. 6b), as would be expected for bacterial sulfate reduction (Clark and Fritz, 1997).

Sr isotopes are sensitive tracers of the interaction of formation waters with specific rocks and minerals with different ages and Rb/Sr, indicating compartmentalization, mixing, and/or transport of fluids (e.g., Stueber et al., 1987; Naftz et al., 1997; Crossey et al., 2006). The Cane Creek brine has the lowest $^{87}Sr/^{86}Sr$ (0.70843) and highest Sr concentration (20.54 mmol/L). The Desert Creek brines have

$^{87}Sr/^{86}Sr$ (0.70845-0.70930) closer to the Cane Creek brine, but have lower Sr concentrations (1.35 to 8.83 mmol/L). $^{87}Sr/^{86}Sr$ of both Cane Creek and Desert Creek brines are close to the values of anhydrite (0.7085; Breit et al., 1990) in the Paradox Fm (Table 4 and Fig. 7). Most of the Honaker Trail Fm brines have high $^{87}Sr/^{86}Sr$ (0.70946-0.71204), comparable to the range of previously reported values for the Permian Cutler Fm waters (0.7094-0.7100; Spangler et al., 1996), but with much higher Sr concentrations (5.70-8.80 mmol/L) than Permian Cutler formation water. The Leadville Ls brine exhibits the highest $^{87}Sr/^{86}Sr$ (0.7175) and contains 1.48 mmol/L of Sr. Brines from the underlying McCracken Ss also show very high $^{87}Sr/^{86}Sr$ (0.71281 and 0.71375) and varied Sr concentrations (2.25 and 7.42 mmol/L). $^{87}Sr/^{86}Sr$ of the salt anticline brine are slightly higher (0.70863-0.70868) with much lower Sr concentrations (0.45-0.49 mmol/L) than those of the Cane Creek brine and anhydrite in the Paradox Fm. The Salt Creek and Dolores River each show a mixing trend toward the salt anticline brine (Fig. 7). For the Dolores River, the mixing trend is composed of meteoric water endmember (DR-BR-a) of 0.01 mmol/L Sr and $^{87}Sr/^{86}Sr$ of 0.7097 and a salt anticline brine endmember of 0.47 mmol/L Sr and $^{87}Sr/^{86}Sr$ of 0.7087 on average. Salt Creek plots on a mixing trend between an estimated meteoric water endmember (PW-11b; groundwater in Navajo Ss) of 0.04 mmol/L Sr and $^{87}Sr/^{86}Sr$ of 0.7097 (dashed line in Fig. 7) and the average salt anticline brine endmember. $^{87}Sr/^{86}Sr$ for groundwater in the Burro Canyon Fm and Navajo Ss correspond to that for hematite, calcite, or barite in Jurassic sandstones (Chan et al., 2000).

Metal (Cu, U, Fe and Mn) and H_2S concentrations in the fluids are summarized in Table 2 and Fig. 8. The maximum Cu concentrations of groundwaters from Cretaceous Burro Canyon and Jurassic Navajo formations is 0.09 μmol/L (Fig. 8a). H_2S in the relatively oxic shallow groundwaters (Noyes et al., 2021) was assumed to be negligible. The Cane Creek brine has the highest Cu concentration (0.48 μmol/L) with moderate H_2S (8.9 mmol/L) within the range of values reported for a spring in California with similar chemistry (Aqua de Ney Spring; 0.47 μmol/L Cu and 11.7 mmol/L H_2S, White, 1963). One of the Honaker Trail Fm brine samples also has detectable Cu (0.44 μmol/L) with moderate H_2S (7.1 mmol/L). Most of the Honaker Trail Fm brine and Desert Creek brine have Cu below the detection limit

(< 0.001 μmol/L) with variable H_2S concentrations. Desert Creek brine has the highest H_2S concentration (14 mmol/L). Leadville Ls brine has Cu contents below the detection limit with high H_2S (8.5 mmol/L) similar to the 0.2 to 1.1 mol % H_2S reported by Paradox Resources (unpublished data). The salt anticline brine contains detectable Cu (0.06-0.09 μmol/L) and high H_2S (5.8-7.1 mmol/L), slightly higher than previously measured by the U.S. Bureau of Reclamation (2.2 mmol/L; unpublished data), but lower Cu and H_2S than the Cane Creek brine.

Uranium concentrations are higher in shallower formation waters compared to deeper fluids (Fig. 8b). Groundwaters in the Burro Canyon Fm have the highest concentration of U (up to 363 nmol/L) with the next highest concentrations found in the Navajo Ss (up to 30 nmol/L). U concentrations at depth decrease in the following order: Honaker Trail Fm brines (up to 8 nmol/L), Cane Creek brine (0.08 nmol/L), and Leadville Ls brine (0.01 nmol/L). Most of Desert Creek brines have low U below the detection limit (< 0.001 nmol/L). The salt anticline brine contains less U compared to the Cane Creek brine.

Most of deep basinal brines have a moderate to high range of Fe and Mn concentrations (Fig. 8c and 8d) with the highest concentrations in the Cane Creek brine (7,185 μmol/L Fe and 1,772 μmol/L Mn). The salt anticline brine contains moderate Fe and Mn concentrations. In contrast, groundwaters in the Burro Canyon, Morrison (Phoenix, 1959) and Navajo Ss formations have a low to moderate range of Fe and Mn concentrations (Table 2).

DISCUSSION

Two Distinct Sources of Salinity in Paradox Basinal Brines

Evaporated Paleo-Seawater-Derived Brine

461 The Cane Creek brine in the Paradox Fm, with lower Cl/Br and Na/Br than seawater (Fig. 4a),
462 high Br and Cl concentrations (Fig. 4b), and the highest $\delta^{18}O_{water}$ and δD_{water} values that plot to the right of
463 the LMWL (Fig. 5), likely formed from subaerial evaporation of seawater, past halite saturation, during
464 the Pennsylvanian, and were deposited with the extensive marine evaporites and shales within the
465 Paradox Fm. The Desert Creek brines in the Paradox Fm also have lower Cl/Br and Na/Br than seawater
466 (Fig. 4a) and high Br and Cl concentrations (Fig. 4b), although not as high as the Cane Creek brine (Fig.
467 4a), indicating they also derived their salinities from evaporated paleo-seawater. The Ca-Cl type brines
468 ($Ca/(SO_4+HCO_3) > 1$; Bein and Dutton, 1993; Hanor and McIntosh, 2006) in the Paradox Fm have
469 similar water stable isotope compositions as fluid inclusions within evaporite minerals (Fig. 5;
470 Petrychenko et al., 2012). The limited previous brine data from the Paradox Fm (Mayhew and Heylmun,
471 1965; Hanshaw and Hill, 1969; Naftz et al., 1997; Blondes et al., 2018) show similar chemistries (e.g., Cl,
472 Na, and Br, Fig. 4) to the Cane Creek brine, while others show similar isotopic compositions (e.g.,
473 $\delta^{18}O_{water}$ and δD_{water}, Fig. 5; $^{87}Sr/^{86}Sr$, Fig. 7) with the Desert Creek brines.

474 The low permeability of the Paradox Fm – a regional confining hydrostratigraphic unit – and high
475 density of residual brines leading to negative buoyancy likely enabled retention of the evaporated paleo-
476 seawater within the Paradox Fm since the Pennsylvanian and prevented it from being completely flushed
477 by meteoric recharge, despite relatively high topographic gradients in the Paradox Basin today (Ferguson
478 et al., 2018). Some portion of these highly saline fluids were likely expelled with hydrocarbons during
479 maximum burial and compaction (Nuccio and Condon, 1996) through faults and fractures (Merin and
480 Segal, 1989) or via diffusion (Hanor and McIntosh, 2007) into adjacent formations. Brines in the
481 Pennsylvanian Honaker Trail Fm contain evidence of evaporated paleo-seawater from the underlying
482 Paradox Fm that was subsequently diluted by meteoric water (Fig. 5 and 9).

483 The high $\delta^{18}O_{water}$ and δD_{water} values of the evaporated paleo-seawater endmember for the
484 Honaker Trail Fm brines plot towards the Paradox Fm Cane Creek brine (Fig 5), while the meteoric water

endmember (corresponding to the intersection of the mixing line with the LWML) has $\delta^{18}O_{water}$ and δD_{water} values consistent with groundwater in the Permian Cutler Fm (Spangler et al., 1996; Fig. 5). Meteoric waters likely circulated through the overlying Permian Cutler Fm, which is part of the same aquifer system (upper hydrostratigraphic unit; Hanshaw and Hill, 1969; Thackston et al., 1981), and mixed with evaporated paleo-seawater to form the Honaker Trail Fm brines.

The Paradox Fm Desert Creek brines also indicate mixing of evaporated paleo-seawater and meteoric influx, but plot on a distinct mixing trend from the Honaker Trail Fm brines with a slightly different saline water endmember (plotting further from seawater, with a lower δD value) (Fig. 5). Differences in the saline endmember isotopic composition may be due to differences in the geographic location of the samples and variations in evaporated paleo-seawater-derived brines within the Paradox Fm. The estimated meteoric water endmember that diluted Desert Creek brines has a relatively high $\delta^{18}O_{water}$ and δD_{water} value (dashed line in Fig. 5), compared to the estimated meteoric water endmember of Honaker Trail Fm brines (dashed line in Fig. 5). This difference in meteoric water endmembers can be attributed to known water injection activity in the Ismay-Desert Creek members of Paradox Fm in the Greater Aneth oil field (Table 1), while there was no water injection activity in the Honaker Trail Fm in the Lisbon Valley area. Together the chemical and isotopic results suggest evaporated paleo-seawater (represented by the Cane Creek brine chemical composition) is one of the major sources of salinity in Paradox Basin brines.

Salt Dissolution-Derived Brines

The salt anticline brine and Mississippian Leadville Ls brines, with higher Cl/Br and Na/Br than seawater (Fig. 4a) and lower Br concentrations than the evaporated seawater line (Fig. 4b), likely derived their salinity from the dissolution of evaporites (e.g., halite) around salt anticline structures or at the base of the Paradox Fm salts, respectively (Fig. 9). The elevated K (Fig. 3) and SO_4 (Fig. 6b) concentrations, relative to evaporated seawater, in the salt anticline and Leadville Ls brines are also consistent with the

dissolution of evaporites (e.g., sylvite, carnallite, kainite, or gypsum). Sr concentrations and $^{87}Sr/^{86}Sr$ of the Dolores River and Salt Creek exhibit a simple binary mixing model between surface waters and salt anticline brine endmember compositions (Fig. 7), consistent with the compositions of surface waters around salt anticline structures controlled by dissolution of salt through meteoric water circulation.

$\delta^{18}O_{water}$ and δD_{water} values of the salt anticline brine and Leadville Ls brines that plot on or close to the LMWL (Fig. 5) confirm meteoric water recharge promoted evaporite dissolution (e.g., McIntosh and Walter, 2005). The $\delta^{18}O_{water}$ and δD_{water} values of the salt anticline brine are comparable to Holocene age (<11 ka based on ^{14}C) groundwater from the Burro Canyon Fm and are distinct from ^{18}O- and D-depleted Late Pleistocene groundwater (15 to 36 ka) from the Navajo Ss (Noyes et al., 2021), suggesting meteoric recharge and salt dissolution around the salt anticlines has occurred since at least the Holocene (e.g., Zhu et al., 2003).

Although both the salt anticline brine and Leadville Ls brine are dominantly derived from dissolution of evaporites, the presence of Br in both brines, above typical concentrations in evaporite minerals (Holser et al., 1979; Kesler et al., 1996), suggests introduction of some component of evaporated paleo-seawater likely associated with the Paradox Fm. The brines in the Leadville Ls have lower Na, K, and Mg concentrations and higher $\delta^{18}O_{water}$ and δD_{water} values further from the LMWL than the salt anticline brine (Fig. 3), suggesting greater contributions of evaporated paleo-seawater in the Leadville Ls brine compared to the salt anticline brine. This is consistent with the PHREEQC inverse mixing model results that show slightly greater contribution of evaporated paleo-seawater in the Leadville Ls brine (4.2 %) compared to the salt anticline brine (2.4 %).

We hypothesize the influx of meteoric waters and salt dissolution are likely a relatively recent phenomenon that followed intrusion of the laccoliths (~28 Ma; Friedman and Huffman, 1997; M. Barton et al., 2018) and denudation of the Colorado Plateau (<10 Ma: Lazear et al., 2011; <4-6 Ma: Murray et al., 2016; Murray et al., 2019), which created higher topographic gradients, removed shale confining units,

and brought the salt anticlines closer to the surface and into contact with meteoric water circulation (Fig. 9). For example, for at least the past ~36 ka (Noyes et al., 2021), topographically-driven meteoric waters has flowed downgradient from the La Sal Mountains through permeable sediments into the Paradox Valley and dissolved evaporites near the top of the salt anticline, which are discharging salt-derived brines into the Dolores River (Chafin et al., 2003; King et al., 2014). Our study results indicate a similar flow system is active in the adjacent Sinbad Valley with discharge of salt anticline-derived brines into Salt Creek, and previous studies have shown similar brine generation mechanisms in Gypsum Valley (Reitman et al., 2014). Meteoric waters recharged around the La Sal and Abajo mountains or along the margins of the salt anticline structures could have flowed into the lower hydrostratigraphic unit (Hanshaw and Hill, 1969; Thackston et al., 1981), underlying the Paradox Fm salts, and may have contributed to the flushing of evaporated paleo-seawater-derived brines (assuming they were present) and generation of more recent evaporite dissolution-derived brines in the Leadville Ls. The flushing of basal aquifers is similar to what was found in the Illinois Basin (Labotka et al., 2015).

Water-Rock Interactions in Basinal Fluids above/below the Paradox Formation

Ca enrichment and Mg and K depletion of the Cane Creek and Desert Creek brines in the Paradox Fm (Fig. 3c and 3d), relative to evaporated seawater (McCaffrey et al., 1987), indicate diagenetic alteration via reaction with siliciclastic and carbonate rocks: e.g., formation of potassium aluminosilicates (Fig. 3b), as well as albitization of plagioclase, saturation with respect to calcite and gypsum (Fig. 3c), and dolomitization (Fig. 3d) (Carpenter, 1978; Hanor, 2001). These diagenetic alterations have been commonly observed in basinal brines at depth in other sedimentary basins, such as the Alberta (Connolly and Walter, 1990), Appalachian (Breen et al., 1985; Lowry et al., 1988; Sanders, 1991), Illinois (Stueber et al., 1993; Stueber and Walter, 1994), and Michigan (Dollar et al., 1991; Wilson and Long, 1993a; 1993b; Martini et al., 1998) basins. We hypothesize these fluid-rock reactions within the Paradox Fm altered the evaporated paleo-seawater derived brines in-situ. As some portion of Paradox Fm brines

557 migrated into over- and under-lying formations they were likely further diagenetically altered (e.g.,
558 Honaker Trail Fm, Leadville Ls and McCracken Fm brines).

559 The radiogenic Sr isotope signatures of basinal brines from the Honaker Trail Fm above the
560 Paradox Fm are consistent with $^{87}Sr/^{86}Sr$ of groundwater in the Permian Cutler Fm (Spangler et al., 1996;
561 Fig. 7) and indicate that the evaporated paleo-seawater-derived brines (mixed with more recent meteoric
562 recharge) in the Honaker Trail Fm have interacted with abundant radiogenic minerals (e.g., alterations of
563 feldspar and micas) of the red, arkosic sandstones (i.e., siliciclastic rocks) in the overlying Cutler and
564 Upper Honaker Trail formations (Breit et al., 1990). The lower K concentration of the Honaker Trail Fm
565 brines compared to the Cane Creek brine (Fig. 3b) may be explained by formation of potassium
566 aluminosilicates by further interaction of brines with siliciclastic rocks within the Honaker Trail Fm. A
567 mixing trend of the Honaker Trail Fm brines in Fig. 6a is evidence of at least two sources of SO_4: 1)
568 oxidation of (^{34}S-depleted) sulfides in the Honaker Trail Fm by influx of meteoric waters and 2)
569 dissolution of (^{34}S-enriched) gypsum associated with the underlying Paradox Fm.

570 The occurrence of the highest $^{87}Sr/^{86}Sr$ in basinal brines from the Mississippian Leadville Ls and
571 Devonian McCracken Ss below the Paradox Fm (Fig. 7), higher than any previously reported
572 measurements of Paradox Basin sediments (Breit et al., 1990; Chan et al., 2000), suggests that the brines
573 have interacted with a highly radiogenic crustal source – likely Precambrian rocks from the Uncompahgre
574 Uplift or crystalline basement beneath the basin (Fig. 9). The Precambrian silicic crystalline rocks from
575 the Uncompahgre Uplift, along the northeastern margin of the basin, have $^{87}Sr/^{86}Sr$ of 0.715-0.735 (Hedge
576 et al., 1968; Mose and Bickford, 1969). Furthermore, the elevated Sr isotope ratios in the Leadville Ls and
577 Devonian McCracken Ss brines are consistent with deeply derived endogenic springs (0.711-0.734
578 $^{87}Sr/^{86}Sr$) in the Grand Canyon region of the Colorado Plateau, that have interacted with Precambrian
579 basement rocks (Crossey et al., 2006). Alternatively, radiogenic Sr in Mississippian Leadville Ls and
580 Devonian McCracken Ss brines could have come from interaction with intervening shale units.

581 Unlike the deeply derived endogenic springs in the Grand Canyon region of the Colorado Plateau
582 (Crossey et al., 2006), most of the brines sampled as part of this study are not CO_2-rich with high
583 alkalinities or DIC (Tables 1 and 3). Three brine samples (TOHO 1, McIntyre 17-21, and Lisbon B8-10)
584 have slightly elevated alkalinities (11.36-12.55 meq/L) and pH (6.78-7.25) values (Table 1), which belong
585 to the range of the endogenic springs. Six brine samples have high calculated DIC values (21.48-42.57
586 meq/L; Table 3), likely dominated by H_2CO_3 at relatively low pH (< 6.5). Potential sources of elevated
587 alkalinity and DIC include influx of mantle CO_2, as seen in the endogenic springs (Crossey et al., 2006;
588 2009), bacterial sulfate reduction (Clark and Fritz, 1997), or decarboxylation (Surdam and MacGowan,
589 1987). Future work using carbon stable isotopes and noble gases are needed to delineate the various
590 sources of alkalinity and DIC.

591 **Paleofluid Flow, Sandstone Bleaching, and Metal Mineralization**

592 ***Relative Redox Conditions***

593 Relative redox conditions for the modern fluids in the Paradox Basin were determined based on
594 the source of water and presence of hydrocarbons and H_2S. Previous studies have shown shallow
595 groundwaters in the Cretaceous Burro Canyon Fm and Jurassic Navajo Ss are oxidized fluids in contact
596 with circulating meteoric waters (Noyes et al., 2021). The salt dissolution-derived brines in the sediments
597 overlying the salt anticlines may be oxidized due to meteoric recharge, but in locations where those salt
598 anticline brine came in contact with black shales there is high H_2S (e.g., Paradox and Sinbad valleys),
599 likely from bacterial sulfate reduction at near-surface temperatures (Clark and Fritz, 1997). The
600 evaporated paleo-seawater-derived brines in the Pennsylvanian Honaker Trail and Paradox formations
601 and salt dissolution-derived brines in the Mississippian Leadville Ls are relatively reduced, as they are
602 associated with hydrocarbons sourced from black shales within the Paradox Fm (Nuccio and Condon,
603 1996). High H_2S concentrations in these formations likely came from thermochemical sulfate reduction
604 (Machel, 2001) associated with gypsum, hydrocarbons, and high maximum burial temperatures (at least

605 120 °C in the Paradox Fm; Nuccio and Condon, 1996). According to the timing of hydrocarbon
606 generation (Nuccio and Condon, 1996), these deep basinal brines have likely been H_2S- and hydrocarbon-
607 bearing reduced fluids since at least the Paleogene (66 to 23 Ma).

608 ***Reduced Fluids Involved in Sandstone Bleaching***

609 Brines from the Pennsylvanian Honaker Trail and Paradox formations were likely a major source
610 of reduced, saline and acidic fluids that were expelled by compaction during maximum burial, ascended
611 along faults, such as the Moab and Lisbon Valley faults, and bleached shallow red-bed sandstones
612 (Entrada Ss, White Rim Ss, Navajo Ss, Wingate Ss). The presence of hydrocarbon residues, such as
613 bitumen, for example in veins between the Page Ss and Entrada Ss along the segment of the Moab fault
614 (Foxford et al., 1998; Hodson et al., 2016) and within the Cutler Fm and Wingate Ss, along the Lisbon
615 Valley anticline, and in the Wingate Ss in the Paradox Valley anticlines (Merin and Segal, 1989; Thorson
616 and MacIntyre, 2005), suggest that acidic reducing brines associated with mobile hydrocarbons were
617 responsible for sandstone bleaching in the Moab fault and the Lisbon and Paradox valley anticlines.

618 Stable isotope and fluid inclusion studies from the faults provide further evidence of the
619 migration of hydrocarbon-associated reducing fluids upward, resulting in the removal of hematite and
620 precipitation of pyrite (Breit et al., 1990; Chan et al., 2000; Garden et al., 2001). The high salinity (5-20
621 wt. %) of fluid inclusions and calculated $\delta^{18}O_{water}$ values (-6.1 to 0.6 ‰) of fluids in carbonate veins
622 (Chinle, Cutler, and Paradox formations) in the Lisbon Valley anticline (Morrison and Parry, 1986) are
623 similar to the salinity (3-26 wt. %) and $\delta^{18}O_{water}$ values of deep basinal brines in the Honaker Trail and
624 Paradox formations, indicating the upward migration of reduced, evaporated paleo-seawater-derived
625 brines along faults. This is further supported by the $\delta^{18}O$ value of carbonate cements (-5 to -0.1‰ VPDB)
626 in the Moab fault having a source fluid composition similar to seawater (Hodson et al., 2016). Although
627 the salt anticline brine with H_2S could have been another potential reducing fluid, the δD and $\delta^{18}O$ values
628 of the salt anticline brine are lower than those of the fluid inclusions in carbonate veins and cements.

Source of Fluids for Cu Mineralization

Presently, there is no clear gradient in Cu concentrations with depth in the Paradox Basin (Fig. 8). If the situation was similar at the time of Cu mineralization, this suggests few constraints on the possible fluid sources involved in Cu mineralization. Shallow sources of Cu could have been immature red beds of the Permian Cutler Fm (Morrison and Parry, 1986) eroded from the Precambrian rock uplift. Alternatively, the deep sources of Cu could have been moderately metal-enriched shales within the Paradox Fm (Tuttle et al., 1996; Thorson, 2018). Compared to the much higher Cu concentrations of Jurassic Morrison Fm groundwaters (0.47 and 1.10 μmol/L, Phoenix, 1959; Fig. 8a), the low Cu concentrations of groundwaters (< 0.09 μmol/L) in the ore-hosting Burro Canyon Fm and Navajo Ss indicate that the abundant supergene Cu minerals are still (meta)stable within the formations in the presence of these relatively oxic meteoric waters.

Although detectable Cu was found in the Paradox Fm Cane Creek brine and one Honaker Trail Fm brine sample, these fluids were unlikely to have been the source of Cu mineralization in shallower sediments as they have likely been reduced H_2S-bearing brines, unsuitable for Cu transport, since the Paleogene or Late Cretaceous (Tuttle et al., 1996; Whidden et al., 2014; Thorson, 2018). This is consistent with the saturation index results showing these fluids are currently supersaturated with respect to CuS and chalcopyrite (Table 3). The salt anticline brine, with similarly high H_2S as deeper brines, has low Cu concentrations (0.06-0.09 μmol/L), and is also unlikely to have transported Cu for mineralization.

It is possible that deeper brines could have been more oxidized in the past prior to hydrocarbon generation and salt anticline-derived brines could have been more oxidized in areas where fluids were not in contact with organic-rich shales. Under these more oxidizing conditions, both types of brines could have acquired ore-forming concentrations of Cu from reaction with Cu-bearing sediments (Sverjensky, 1987). Calcite associated with Cu minerals in Lisbon Valley has a small range of $\delta^{18}O$ values that is consistent with precipitation in equilibrium with residual marine or isotopically evolved meteoric water

(Breit and Meunier, 1990), suggesting that upwelling of evaporated paleo-seawater along faults may have been associated with Cu mineralization. However, hydrocarbon-bearing reduced fluids preceded Cu mineralization to provide a reduced trap for the Cu (Hahn and Thorson, 2006; Thorson, 2018). In addition to this, if a deeper fluid like the Paradox Fm Cane Creek brine, with 0.48 μmol/L Cu, formed the 62 x 10^9 kg Cu deposit of the Lisbon Valley (Hahn and Thorson, 2006), it would have required approximately 4.6 x 10^{13} m^3 of brine to have been driven upwards along a fault during maximum burial. This flux of Cu-bearing fluid from the Paradox Fm is unlikely given its low permeability and relatively short time period of maximum burial and upward flow driven by compaction. Therefore, regional flow driven by topographic gradients or more localized thermo-haline convection-driven circulation are more likely to have delivered Cu for mineralization from near-surface source(s). The requirement of an initial flux of saline, reduced, acidic fluids followed by more oxic Cu-bearing fluids represents an emergent behavior, where a certain sequence of independent events is required to create a Cu-deposit.

Sources of Fluids for U Mineralization

Unlike Cu, there is a clear decrease in U concentrations with depth in the Paradox Basin (Fig. 8b), suggesting a near-surface source of U for U mineralization within the Jurassic Morrison and Triassic Chinle and other formations or more reducing conditions with depth (Thorson, 2018), assuming the situation was similar at the time of U mineralization. U is immobile under relatively reduced conditions (Langmuir, 1978). Consequently, although the black shale within the Paradox Fm has a high U content (~70 ppm; Thorson, 2018), little of that U is likely to be mobilized in the hydrocarbon and H_2S-associated, evaporated paleo-seawater-derived brines associated with the Paradox Fm.

Another potential U source is granitic debris derived from the U-enriched Precambrian rocks of the Uncompahgre Uplift (Thamm et al., 1981; Thorson, 2018). Relatively oxic meteoric waters could have interacted with the granitic debris in the shallower clastic sediments and transported U into adjacent units. Previous studies have suggested that tuffaceous volcanic materials in the Morrison and Chinle

677 formations were also a potential source of U (Waters et al., 1949; Christiansen et al., 2015).
678 Groundwaters in the Morrison Fm contain very high U concentrations (84-75,621 nmol/L, Phoenix, 1959;
679 Fig. 8b). However, sufficiently high fluid fluxes through the low-permeability Brushy Basin shale
680 member of the Morrison Fm are unlikely to have occurred and there are no known U deposits in
681 tuffaceous regions of the Morrison Fm.

682 Although reduced fluids were unlikely to have been the source of U, they may have played a role
683 in providing a trap for U mineralization. Most historical interpretations have attributed U reduction and
684 precipitation to solid reducing matter, such as coalified plant trash, or to humate or other dissolved species
685 emanating from decomposing plant materials. While high-grade zones can localize around solid
686 reductants, the overall relationship between known plant and animal remains and U-V concentrations is
687 inconsistent (Shawe, 2011). Recent findings of remnant hydrocarbons in Chinle- and Salt Wash-hosted
688 deposits indicate that hydrocarbon-associated fluids, such as the Paradox Fm brines, may have
689 contributed to U-V mineralization – although as reducing traps rather than metal sources (I. Barton et al.,
690 2018).

691 **CONCLUSIONS**

692 Synthesizing the various chemical and isotopic tracers, we found that highly evaporated paleo-
693 seawater-derived brines are retained within the Pennsylvanian Paradox Fm (containing evaporites) with
694 no evidence of meteoric water flushing. Some portion of these reduced, saline fluids were likely expelled
695 with hydrocarbons into overlying formations during maximum burial, ascending through faults, bleaching
696 former red bed Cretaceous and Jurassic sandstones, and precipitating reduced minerals, consistent with
697 the presence of some component of evaporated paleo-seawater within the Honaker Trail Fm. Honaker
698 Trail Fm brines were further modified by reaction with radiogenic siliciclastic minerals. Cu was unlikely
699 to have been sourced from metal-rich black shales in the Paradox Fm and co-transported with brines into
700 shallower formations due to high H_2S concentrations and insufficient fluid fluxes from these deep units.

Salt dissolution-derived brines were identified around salt anticlines and underlying the base of the Paradox Fm evaporites. The shallow salt dissolution-derived brines were also unlikely to have transported Cu due to high H_2S concentrations from bacterial sulfate reduction. The relatively recent intrusion of laccoliths (28 Ma) and denudation (<4-10 Ma) of this part of the Colorado Plateau likely setup a more active topographically-driven flow system that resulted in deeper meteoric water circulation, flushing of evaporated paleo-seawater-derived brines in the basal units, and dissolution of evaporites above and below the Paradox Fm salts. Relatively high $^{87}Sr/^{86}Sr$ of formation waters in the Mississippian and Devonian aquifers suggests circulation of fluids through radiogenic Precambrian rocks from the Uncompahgre Uplift or underlying crystalline basement and/or intervening shales in basal sediments.

Meteoric circulation of more oxic waters contributed to high U concentrations of groundwater in the Burro Canyon Fm, Morrison Fm, and Navajo Ss, compared to deep, reduced brines, indicating a near-surface source for U mineralization, if the hydrochemical stratigraphic configuration was similar at the time of U mineralization. Hydrocarbons and other reduced materials introduced into formerly oxidized units likely provided a trap for U carried by later, oxidized, fluids. Similarly, circulation of oxic waters through Cu-enriched shallow red beds eroded from the Precambrian rock uplift was likely responsible for Cu transport and subsequent Cu mineralization in areas of residual bitumen and/or reduced minerals.

Multiple sequential episodes of paleofluid flow from different sources and subsequent fluid-rock reactions were required to explain the emergent behavior of sandstone bleaching by a reduced saline fluid, and ore mineralization likely by circulation of more oxic, saline waters across the Colorado Plateau. Further investigation of the timing of regional groundwater flow and flushing of residual brines is needed to constrain the timescales, pathways and drivers of paleofluid flow.

ACKNOWLEDGEMENTS

Funding for this research was provided by the W.M. Keck Foundation, CIFAR Earth4D Subsurface Science and Exploration program, and NSF EAR (#2120733). The authors would like to acknowledge the U.S. Bureau of Reclamation, Paradox Resources, Navajo Petroleum, US Oil and Gas INC, Anson Resources, Lantz Indergard (Lisbon Valley Mining Co.), Ambria Dell'Oro, and Mohammad Marza for help with sampling. Dr. Steven Lingrey provided insights on stratigraphy in the Paradox Basin. Tim Corley provided laboratory assistance. The authors also would like to acknowledge the Associate Editor and reviewers (Drs. Laura Crossey, Jean-Philippe Nicot, and Ipsita Gupta) for their significant comments that greatly improved the manuscript.

REFERENCES CITED

Achtziger-Zupančič, P., Loew, S., and Mariethoz, G., 2017, A new global database to improve predictions of permeability distribution in crystalline rocks at site scale: Journal of Geophysical Research: Solid Earth, v. 122, no. 5, p. 3513-3539.

Ake, J., Mahrer, K., O'Connell, D., and Block, L., 2005, Deep-injection and closely monitored induced seismicity at Paradox Valley, Colorado: Bulletin of the Seismological Society of America, v. 95, no. 2, p. 664-683.

Appelo, C. A. J., and Postma, D., 2004, Geochemistry, groundwater and pollution, AA Balkema, Rotterdam, The Netherlands.

Baars, D. L., 1966, Pre-Pennsylvanian paleotectonics—Key to basin evolution and petroleum occurrences in Paradox Basin, Utah and Colorado: American Association of Petroleum Geologists Bulletin, v. 50, no. 10, p. 2082-2111.

Baars D. L., and Stevenson G. M., 1982, Subtle stratigraphic traps in Paleozoic rocks of Paradox Basin, *in* Halbouty, M. T., ed., The Deliberate Search for the Subtle Trap: American Association of Petroleum Geologists Memoir, 32, p. 131-158.

Back W., Hanshaw B. B., Plummer L. N., Rahn P. H., Rightmire C. T., and Rubin M., 1983, Process and rate of dedolomitization: mass transfer and ^{14}C dating in a regional carbonate aquifer: Geological Society of America Bulletin, v. 94, no. 12, p.1415-1429.

Barbeau, D. L., 2003, A flexural model for the Paradox Basin: implications for the tectonics of the Ancestral Rocky Mountains: Basin Research, v. 15, no. 1, p. 97-115.

Barton I., Barton M. D., and Thorson J., 2018, Characteristics of Cu and UV Deposits in the Paradox Basin (Colorado Plateau) and Associated Alteration: Society of Economic Geologists, Guidebook series, v. 59, p. 73-102.

Barton, M. D., Barton, I., and Thorson, J., 2018, Paleofluid Flow in the Paradox Basin: Introduction: Society of Economic Geologists, Guidebook series, v. 59, p. 1-12.

Bein, A., and Dutton, A. R., 1993, Origin, distribution, and movement of brine in the Permian Basin (USA): A model for displacement of connate brine: Geological Society of America Bulletin, v. 105, no. 6, p. 695-707.

Beauheim, R. L., Roberts, R. M., Dale, T. F., Fort, M. D., and Stensrud, W. A., 1993, Hydraulic Testing of Salado Formation Evaporites at the Waste Isolation Pilot Plant Site: Second Interpretive Report, Sandia National Laboratory, no. SAND-92-0533.

Bethke, C. M., and Marshak, S., 1990, Brine migrations across North America-the plate tectonics of groundwater: Annual Review of Earth and Planetary Sciences, v. 18, p. 287-315.

Blondes, M.S., Gans, K.D., Engle, M.A., Kharaka, Y.K., Reidy, M.E., Saraswathula, V., Thordsen, J.J., Rowan, E.L., and Morrissey, E.A., 2018, U.S. Geological Survey National Produced Waters Geochemical Database: U.S. Geological Survey data release, ver. 2.3, January.

Breen, K. J., 1985, Chemical and isotopic characteristics of brines from three oil-and gas-producing sandstones in eastern Ohio, with applications to the geochemical tracing of brine sources: U.S. Geological Survey Water-Resources Investigations Report, no. 84-4314, 58 p.

Breit, G. N., and Meunier, J. D., 1990, Fluid inclusion, $\delta^{18}O$, and $^{87}Sr/^{86}Sr$ evidence for the origin of fault-controlled copper mineralization, Lisbon Valley, Utah, and Slick Rock District, Colorado: Economic Geology, v. 85, no. 4, p. 884-891.

Breit G. N., Goldhaber M. B., Shawe D. R., and Simmons E. C., 1990, Authigenic barite as an indicator of fluid movement through sandstones within the Colorado Plateau: Journal of Sedimentary Research, v. 60, no. 6, p. 884-896.

Bremkamp, W., and Harr, C. L., 1988, Area of least resistance to fluid movement and pressure rise: Paradox Valley Unit, Salt Brine Injection Project, Bedrock, Colorado: a report prepared for the U.S. Bureau of Reclamation, Denver, Colorado, 39.

Carpenter, A. B., 1978, Origin and chemical evolution of brines in sedimentary basins: In SPE Annual Fall Technical Conference and Exhibition, Society of Petroleum Engineers, January.

Cater, F. W., and Craig, L. C., 1970, Geology of the salt anticline region in southwestern Colorado: U.S. Geological Survey Professional Paper, no. 637, 80 p.

Chafin D. T., 2003, Effect of the Paradox Valley Unit on the dissolved-solids load of the Dolores River near Bedrock, Colorado, 1988-2001: U.S. Geological Survey Water-Resources Investigations Report, no. 2-4275.

Chan M. A., Parry W. T., and Bowman J. R., 2000, Diagenetic hematite and manganese oxides and fault-related fluid flow in Jurassic sandstones, southeastern Utah: American Association of Petroleum Geologists Bulletin, v. 84, no. 9, p. 1281-1310.

Chen F., Turchyn A. V., Kampman N., Hodell D., Gázquez F., Maskell A., and Bickle M., 2016, Isotopic analysis of sulfur cycling and gypsum vein formation in a natural CO_2 reservoir: Chemical Geology, v. 36, p. 72-83.

792 Christensen, E. H., Kowallis, B. J., and Barton, M. D., 1994, Temporal and spatial distribution of volcanic
793 ash in Mesozoic sedimentary rocks of the western interior: An alternative record of Mesozoic
794 magmatism, *in* Caputo, M.V., Peterson, J.A., and Franczyk K.J., eds., Mesozoic Systems of the
795 Rock Mountain Region, USA: Rocky Mountain Section [SEPM], p. 73-94.

796 Christiansen E. H., Kowallis B. J., Dorais M. J., Hart G. L., Mills C. N., Pickard M., and Parks, E., 2015,
797 The record of volcanism in the Brushy Basin Member of the Morrison Formation: Implications
798 for the Late Jurassic of western North America: Geological Society of America Special Paper, v.
799 513, p. 399-439.

800 Clark I. D., and Fritz P., 1997, Environmental isotopes in hydrogeology: CRC press, Boca Raton, 328 p.

801 Connolly, C. A., Walter, L. M., Baadsgaard, H., and Longstaffe, F. J., 1990, Origin and evolution of
802 formation waters, Alberta basin, western Canada sedimentary basin. I. Chemistry: Applied
803 Geochemistry, v. 5, no. 4, p. 375-395.

804 Craig, H., 1961, Isotopic variations in meteoric waters: Science, v. 133, no. 3465, p. 1702-1703.

805 Crossey L. J., Fischer T. P., Patchett P. J., Karlstrom K. E., Hilton D. R., Newell D. L., Huntoon P.,
806 Reynolds A. C., and De Leeuw, G. A., 2006, Dissected hydrologic system at the Grand Canyon:
807 Interaction between deeply derived fluids and plateau aquifer waters in modern springs and
808 travertine: Geology, v. 34, no. 1, p. 25-28.

809 Crossey L. J., Karlstrom K. E., Springer A. E., Newell D., Hilton D. R., and Fischer T., 2009, Degassing
810 of mantle-derived CO_2 and He from springs in the southern Colorado Plateau region—
811 Neotectonic connections and implications for groundwater systems: Geological Society of
812 America Bulletin, v. 121, no. 7-8, p. 1034-1053.

813 Doelling, H. H., 1988, Geology of Salt Valley anticline and Arches National Park, Grand County, Utah.
814 Salt deformation in the Paradox region, Utah: Utah Geological and Mineral Survey Bulletin, v.
815 122, p. 1-60.

816 Dollar, P. S., Frape, S. K., and McNuff, R. H., 1991, Geochemistry of formation waters, southwestern
817 Ontario, Canada and southern Michigan, USA: Implications for origin and evolution: Queen's
818 Printer for Ontario.

819 Engle M. A., Reyes F. R., Varonka M. S., Orem W. H., Ma L., Ianno A. J., Schell T. M., Xu P., and
820 Carroll, K. C., 2016, Geochemistry of formation waters from the Wolfcamp and "Cline" shales:
821 Insights into brine origin, reservoir connectivity, and fluid flow in the Permian Basin,
822 USA: Chemical Geology, v. 425, p. 76-92.

823 Ferguson, G., McIntosh, J. C., Grasby, S. E., Hendry, M. J., Jasechko, S., Lindsay, M. B., and Luijendijk,
824 E., 2018, The persistence of brines in sedimentary basins: Geophysical Research Letters, v. 45,
825 no. 10, p. 4851-4858.

826 Foxford, K. A., Walsh, J. J., Watterson, J., Garden, I. R., Guscott, S. C., and Burley, S. D., 1998,
827 Structure and content of the Moab Fault Zone, Utah, USA, and its implications for fault seal
828 prediction: Geological Society, London, Special Publications, v. 147, no. 1, p. 87-103.

829 Friedman, J.D., and Huffman, A.C., 1997, Laccolith complexes of southeastern Utah: Time of
830 emplacement and tectonic setting: U.S. Geological Survey, Bulletin, no. 2158.

831 Garcia V. H., Reiners P. W., Shuster D. L., Idleman B., and Zeitler, P. K., 2018, Thermochronology of
832 sandstone-hosted secondary Fe-and Mn-oxides near Moab, Utah: Record of paleo–fluid flow
833 along a fault: Geological Society of America Bulletin, v. 130, no. 1-2, p. 93-113.

834 Garden, I. R., Guscott, S. C., Burley, S. D., Foxford, K. A., Walsh, J. J., and Marshall, J., 2001, An
835 exhumed palaeo-hydrocarbon migration fairway in a faulted carrier system, Entrada Sandstone of
836 SE Utah, USA: Geofluids, v. 1, no. 3, p. 195-213.

837 Gardner, P. M., Nelson, N. C., Heilweil, V. M., Solder, J. E., and Solomon, D. K., 2020, Rethinking a
838 groundwater flow system using a multiple-tracer geochemical approach: A case study in Moab-
839 Spanish Valley, Utah: Journal of Hydrology, v. 590, no. 125512.

840 Garven, G., 1989, A hydrogeologic model for the formation of the giant oil sands deposits of the Western
841 Canada sedimentary basin: American Journal of Science, v. 289, no. 2, p. 105-166.

842 Gieskes, J. M., and Rogers, W. C., 1973, Alkalinity determination in interstitial waters of marine
843 sediments: Journal of sedimentary research, v. 43, no. 1, p. 272-277.

844 Grasby, S. E., and Chen, Z., 2005, Subglacial recharge into the Western Canada Sedimentary Basin—
845 Impact of Pleistocene glaciation on basin hydrodynamics: Geological Society of America
846 Bulletin, v. 117, no. 3-4, p. 500-514.

847 Gupta I., Wilson A. M., and Rostron B. J., 2012, Cl/Br compositions as indicators of the origin of brines:
848 Hydrogeologic simulations of the Alberta Basin, Canada: Geological Society of America
849 Bulletin, v. 124, no. 1-2, p. 200-212.

850 Hahn, G. A., and Thorson, J. P., 2006, Geology of the Lisbon Valley sandstone-hosted disseminated
851 copper deposits, San Juan County, Utah: Utah Geological Association Publication, v. 32, p. 511–
852 533

853 Hanor J. S., 2001, Reactive transport involving rock-buffered fluids of varying salinity: Geochimica et
854 Cosmochimica Acta, v. 65, no. 21, p. 3721-3732.

855 Hanor, J. S., and McIntosh, J. C., 2006, Are secular variations in seawater chemistry reflected in the
856 compositions of basinal brines?: Journal of Geochemical Exploration, v. 89, no. 1-3, p. 153-156.

857 Hanor, J. S., and McIntosh, J. C., 2007, Diverse origins and timing of formation of basinal brines in the
858 Gulf of Mexico sedimentary basin: Geofluids, v. 7, no. 2, p. 227-237.

859 Hanshaw B. B., and Hill G. A., 1969, Geochemistry and hydrodynamics of the Paradox basin region,
860 Utah, Colorado and New Mexico: Chemical Geology, v. 4, no. 1-2, p. 263-294.

861 Hanshaw B. B., Back W., and Deike R. G., 1971, A geochemical hypothesis for dolomitization by ground
862 water: Economic Geology, v. 66, no. 5, p. 710-724.

863 Hartley, A., and Evenstar, L., 2018, Fluvial architecture in actively deforming salt basins: Chinle
864 Formation, Paradox Basin, Utah: Basin Research, v. 30, no. 1, p. 148-166.

865 Hedge, C. E., Peterman, Z. E., Case, J. E., and Obradovich, J. D., 1968, Precambrian geochronology of
866 the northwestern Uncompahgre Plateau, Utah and Colorado: U.S. Geological Survey Professional
867 Paper, no. 600, p. C91-96.

868 Hite R. J., Anders D. E., and Ging T. G., 1984, Organic-rich source rocks of Pennsylvanian age in the
869 Paradox Basin of Utah and Colorado, *in* Woodward, J., Meissner F.F., and Clayton J.L., eds.,
870 Hydrocarbon Source Rocks of the Greater Rocky Mountain Region: Rocky Mountain Association
871 of Geologists, Denver, Colorado, p. 255-274.

872 Hite, R.J., and Buckner, D.H., 1981, Stratigraphic correlations, facies concepts, and cyclicity in
873 Pennsylvanian rocks of the Paradox basin, *in* Wiegand D.L. ed., Geology of the Paradox Basin:
874 Rocky Mountain Association of Geologists, p. 147-159.

875 Hite R. J., and Lohman S. W., 1973, Geologic appraisal of Paradox basin salt deposits for water
876 emplacement: U.S. Geological Survey Open-File Report, No. 73-114 (4339–6).

877 Hodson, K. R., Crider, J. G., and Huntington, K. W., 2016, Temperature and composition of carbonate
878 cements record early structural control on cementation in a nascent deformation band fault zone:
879 Moab Fault, Utah, USA: Tectonophysics, v. 690, p. 240-252.

880 Holt N. M., García-Veigas J., Lowenstein T. K., Giles P. S., and Williams-Stroud S., 2014, The major-ion
881 composition of Carboniferous seawater: Geochimica et Cosmochimica Acta, v. 134, p. 317-334.

882 Kendall, C., and Coplen, T. B., 2001, Distribution of oxygen-18 and deuterium in river waters across the
883 United States: Hydrological processes, v. 15, no. 7, p. 1363-1393.

884 Kharaka, Y. K., Ambats, G., Thordsen, J. J., and Davis, R. A., 1997, Deep well injection of brine from
885 Paradox Valley, Colorado: Potential major precipitation problems remediated by
886 nanofiltration: Water resources research, v. 33, no. 5, p. 1013-1020.

887 Kharaka, Y. K., and Hanor, J. S., 2003, Deep fluids in the continents: I. Sedimentary basins: Treatise on
888 geochemistry, v. 5, p. 1-48.

889 Kharaka, Y. K., Maest, A. S., Carothers, W. W., Law, L. M., Lamothe, P. J., and Fries, T. L., 1987,
890 Geochemistry of metal-rich brines from central Mississippi Salt Dome basin, USA: Applied
891 Geochemistry, v. 2, no. 5-6, p. 543-561.

892 King V. M., Block L. V., Yeck W. L., Wood C. K., and Derouin, S. A., 2014, Geological structure of the
893 Paradox Valley Region, Colorado, and relationship to seismicity induced by deep well
894 injection: Journal of Geophysical Research: Solid Earth, v. 119, no. 6, p. 4955-4978.

895 Kotzer T. G., and Kyser T. K., 1995, Petrogenesis of the Proterozoic Athabasca Basin, northern
896 Saskatchewan, Canada, and its relation to diagenesis, hydrothermal uranium mineralization and
897 paleohydrogeology: Chemical Geology, v. 120, no. 1-2, p. 45-89.

898 Labotka, D. M., Panno, S. V., Locke, R. A., and Freiburg, J. T., 2015, Isotopic and geochemical
899 characterization of fossil brines of the Cambrian Mt. Simon Sandstone and Ironton–Galesville
900 Formation from the Illinois Basin, USA: Geochimica et Cosmochimica Acta, v. 165, p. 342-360.

901 Langmuir, D., 1978, Uranium solution-mineral equilibria at low temperatures with applications to
902 sedimentary ore deposits: Geochimica et Cosmochimica Acta, v. 42, no. 6, p. 547-569.

903 Lazear, G. D., Karlstrom, K. E., Aslan, A., Schmandt, B., Beard, L. S., and CREST Working Group,
904 2011, Denudational flexural isostasy of the Colorado Plateau: Implications for incision rates and
905 tectonic uplift, *in* Beard, L.S., Karlstrom, K. E., Young, R. A., and Billingsley, G. H., eds., C

Revolution 2—Origin and Evolution of the Colorado River System, Workshop Abstracts: U.S. Geological Survey Open-File Report 2011-1210, p. 287-295.

Lawton, T. F., and Buck, B. J., 2006, Implications of diapir-derived detritus and gypsic paleosols in Lower Triassic strata near the Castle Valley salt wall, Paradox Basin, Utah: Geology, v. 34, no. 10, p. 885-888.

Lawton, T. F., Buller, C. D., and Parr, T. R., 2015, Provenance of a Permian erg on the western margin of Pangea: Depositional system of the Kungurian (late Leonardian) Castle Valley and White Rim sandstones and subjacent Cutler Group, Paradox Basin, Utah, USA: Geosphere, v. 11, no. 5, p. 1475-1506.

Leary, R. J., Umhoefer, P., Smith, M. E., and Riggs, N., 2017, A three-sided orogen: A new tectonic model for Ancestral Rocky Mountain uplift and basin development: Geology, v. 45, no. 8, p. 735-738.

Loope D. B., Kettler R. M., and Weber K. A., 2010, Follow the water: Connecting a CO_2 reservoir and bleached sandstone to iron-rich concretions in the Navajo Sandstone of south-central Utah, USA: Geology, v. 38, no. 11, p. 999-1002.

Lowry, R. M., Faure, G., Mullet, D. I., and Jones, L. M., 1988, Interpretation of chemical and isotopic compositions of brines based on mixing and dilution, "Clinton" sandstones, eastern Ohio, USA: Applied geochemistry, v. 3, no. 2, p. 177-184.

Machel H. G., 1999, Effects of groundwater flow on mineral diagenesis, with emphasis on carbonate aquifers: Hydrogeology Journal, v. 7, no. 1, p. 94-107.

Machel, H. G., 2001, Bacterial and thermochemical sulfate reduction in diagenetic settings—old and new insights: Sedimentary Geology, v. 140, no. 1-2, p. 143-175.

Martini, A. M., Walter, L. M., Budai, J. M., Ku, T. C., Kaiser, C. J., and Schoell, M., 1998, Genetic and temporal relations between formation waters and biogenic methane: Upper Devonian Antrim Shale, Michigan Basin, USA: Geochimica et Cosmochimica Acta, v. 62, no. 10, p. 1699-1720.

Mayhew, E. J., and Heylmun, E. B., 1965, Concentrated Subsurface Brines in the Moab Region, Utah: Utah Geological and Mineralogical Survey Special Studies, v. 13, p. 28.

McBride, E. F., 2016, Stratigraphy, petrography, and depositional history of the Ignacio Quartzite and McCracken Sandstone Member of the Elbert Formation, southwestern Colorado, USA: Rocky Mountain Geology, v. 51, no. 2, p. 23-68.

McCaffrey, M. A., Lazar, B. H. D. H., and Holland, H. D., 1987, The evaporation path of seawater and the coprecipitation of Br^- and K^+ with halite: Journal of Sedimentary Research, v. 57, no. 5, p. 928-937.

McIntosh, J. C., and Walter, L. M., 2005, Volumetrically significant recharge of Pleistocene glacial meltwaters into epicratonic basins: Constraints imposed by solute mass balances: Chemical Geology, v. 222, no. 3-4, p. 292-309.

McIntosh, J. C., Walter, L. M., and Martini, A. M., 2002, Pleistocene recharge to midcontinent basins: effects on salinity structure and microbial gas generation: Geochimica et Cosmochimica Acta, v. 66, no. 10, p. 1681-1700.

Merin I. S., and Segal D. B., 1989, Diagenetic alteration of the Wingate Formation: Possible indications of hydrocarbon microseepage, Lisbon Valley, Utah: The Journal of Geology, v. 97, no. 6, p. 719-734.

Morrison, S. J., and Parry, W. T., 1986, Formation of carbonate-sulfate veins associated with copper ore deposits from saline basin brines, Lisbon Valley, Utah; fluid inclusion and isotopic evidence: Economic Geology, v. 81, no. 8, p. 1853-1866.

Mose, D. G., and Bickford, M. E., 1969, Precambrian geochronology in the Unaweep Canyon, west-central Colorado: Journal of Geophysical Research, v. 74, no. 6, p. 1677-1687.

Murray, K. E., Reiners, P. W., and Thomson, S. N., 2016, Rapid Pliocene–Pleistocene erosion of the central Colorado Plateau documented by apatite thermochronology from the Henry Mountains: Geology, v. 44, no. 6, p. 483-486.

Murray, K. E., Reiners, P. W., Thomson, S. N., Robert, X., and Whipple, K. X., 2019, The thermochronologic record of erosion and magmatism in the Canyonlands region of the Colorado Plateau: American Journal of Science, v. 319, no. 5, p. 339-380.

Naftz D. L., Peterman Z. E., and Spangler, L. E., 1997, Using $\delta^{87}Sr$ values to identify sources of salinity to a freshwater aquifer, Greater Aneth Oil Field, Utah, USA: Chemical Geology, v. 141, no. 3-4, p. 195-209.

Northrop H. R., Goldhaber M. B., Landis G. P., Unruh J. W., Reynolds R. L., Campbell J. A., Wanty R. B., Grauch R. I., Whitney G., Landis G. P., and Rye R. O., 1990, Genesis of the tabular-type vanadium-uranium deposits of the Henry Basin, Utah: Economic Geology, v. 85, no. 2, p. 215-269.

Noyes, C., Kim, J., Person, M., Ma, L., Ferguson, G., and McIntosh, J. C., 2021, A geochemical and isotopic assessment of hydraulic connectivity of a stacked aquifer system in the Lisbon Valley, Utah (USA), and critical evaluation of environmental tracers: Hydrogeology Journal, p. 1-19.

Nuccio V. F., and Condon S. M., 1996, Burial and thermal history of the Paradox Basin, Utah and Colorado, and petroleum potential of the middle Pennsylvanian Paradox Formation: U.S. Geological Survey Bulletin 2000-O, 41 p.

Nuckolls, H. M., and McCulley, B. L., 1987, Origin of saline springs in Cataract Canyon, Utah, *in* Campbell, J. A., ed., Geology of Cataract Canyon and vicinity: Four Corners Geological Society, 10th Field Conference, Guidebook, p. 193–199.

Petrychenko, Y., Williams-Stroud, S., and Peryt, T. M., 2012, The relationship of brine chemistry of the Pennsylvanian Paradox Evaporite Basin (southwestern USA) to secular variation in seawater chemistry: Geological Quarterly, v. 56, no. 1, p. 25-40.

Phoenix, D. A., 1959, Part 4. Occurrence and chemical character of ground water in the Morrison Formation: U.S. Geological Survey Professional Paper, no. 320, p. 55-64.

Plummer, L. N., 1988, A computer program incorporating Pitzer's equations for calculation of geochemical reactions in brines: Department of the Interior, U.S. Geological Survey, v. 88, no. 4153.

Reiners, P. W., Chan, M. A., and Evenson, N. S., 2014, (U-Th)/He geochronology and chemical compositions of diagenetic cement, concretions, and fracture-filling oxide minerals in Mesozoic sandstones of the Colorado Plateau: Geological Society of America Bulletin, v. 126, no. 9-10, p. 1363-1383.

Reitman, N. G., Ge, S., and Mueller, K., 2014, Groundwater flow and its effect on salt dissolution in Gypsum Canyon watershed, Paradox Basin, southeast Utah, USA: Hydrogeology Journal, v. 22, no. 6, p. 1403-1419.

Riley, J. P., and Chester, R., 1971, Introduction to marine chemistry: Academic, New York.

Rose, A.W., 1989. Mobility of copper and other heavy metals in sedimentary environments, *in* Boyle, R.W., Brown, A.C., Jefferson, C.W., Jowett, E.C., and Kirkham, R.V., eds., Sediment-Hosted Stratiform Copper Deposits: Geological Association of Canada, Special Paper, v. 36, p. 97–110.

Rose A. W., and Bianchi-Mosquera G. C., 1993, Adsorption of Cu, Pb, Zn, Co, Ni, and Ag on goethite and hematite; a control on metal mobilization from red beds into stratiform copper deposits: Economic Geology, v. 88, no. 5, p. 1226-1236.

Rosenbauer, R. J., Bischoff, J. L., and Kharaka, Y. K., 1992, Geochemical effects of deep-well injection of the Paradox Valley brine into Paleozoic carbonate rocks, Colorado, USA: Applied geochemistry, v. 7, no. 3, p. 273-286.

Sanders, L. L., 1991, Geochemistry of formation waters from the lower Silurian Clinton formation (Albion sandstone), eastern Ohio: American Association of Petroleum Geologists Bulletin, v. 75, no. 10, p. 1593-1608.

Sanford R. F., 1990a, Paleo hydrogeology of the Colorado Plateau-background and conceptual models: The Geochemical Society Special Publication, no. 2, p. 285-311.

Sanford, R. F., 1990b, Hydrogeology of an ancient arid closed basin: Implications for tabular sandstone-hosted uranium deposits: Geology, v. 18, no. 11, p. 1099-1102.Sanford R. F., 1992, A new model for tabular-type uranium deposits: Economic Geology, v. 87, no. 8, p. 2041-2055.

Sanford R. F., 1994, A quantitative model of ground-water flow during formation of tabular sandstone uranium deposits: Economic Geology, v. 89, no. 2, p. 341-360.

Shawe, D. R., 1968, Petrography of Sedimentary Rocks in the Slick Rock District, San Miguel and Dolores Counties, Colorado. U.S. Geological Survey Professional Paper, no. 576-B, 34 p.

Shawe D. R., 2011, Uranium-vanadium deposits of the Slick Rock district, Colorado. U.S. Geological Survey Professional Paper, no. 576-F, 80 p.

Sofer, Z., and Gat, J. R., 1972, Activities and concentrations of oxygen-18 in concentrated aqueous salt solutions: analytical and geophysical implications: Earth and Planetary Science Letters, v. 15, no. 3, p. 232-238.

1017 Sofer, Z., and Gat, J. R., 1975, The isotope composition of evaporating brines: effect of the isotopic
1018 activity ratio in saline solutions: Earth and Planetary Science Letters, v. 26, no. 2, p. 179-186.

1019 Spangler L. E., Naftz D. L., and Peterman, Z. E., 1996, Hydrology, chemical quality, and characterization
1020 of salinity in the Navajo aquifer in and near the Greater Aneth Oil Field, San Juan County, Utah:
1021 U.S. Geological Survey Water-Resources Investigations Report, no. 96-4155, 90 p.

1022 Stanton, J. S., Anning, D. W., Brown, C. J., Moore, R. B., McGuire, V. L., Qi, S. L., Harris A. C.,
1023 Dennehy K. F., McMahon P. B., Degnan J. R., and Böhlke, J. K., 2017, Brackish groundwater in
1024 the United States: U.S. Geological Survey Professional Paper, no. 1833, 202 p.

1025 Stevenson, G. M., and Baars, D. L., 1986, The Paradox: A Pull-Apart Basin of Pennsylvanian Age, *in*
1026 Peterson, J.E. ed., Palcotectonics and Sedimentation in the Rocky Mountain Region, United
1027 States: American Association of Petroleum Geologists Memoir, 41, p. 513-539.

1028 Stober, I., and Bucher, K., 2007, Hydraulic properties of the crystalline basement: Hydrogeology Journal,
1029 v. 15, no. 2, p. 213-224.

1030 Stueber A. M., Pushkar P., and Hetherington E. A., 1987, A strontium isotopic study of formation waters
1031 from the Illinois basin, USA: Applied Geochemistry, v. 2, no. 5-6, p. 477-494.

1032 Stueber, A. M., Walter, L. M., Huston, T. J., and Pushkar, P., 1993, Formation waters from
1033 Mississippian-Pennsylvanian reservoirs, Illinois basin, USA: Chemical and isotopic constraints
1034 on evolution and migration: Geochimica et Cosmochimica Acta, v. 57, no. 4, p. 763-784.

1035 Stueber, A. M., and Walter, L. M., 1994, Glacial recharge and paleohydrologic flow systems in the
1036 Illinois basin: Evidence from chemistry of Ordovician carbonate (Galena) formation
1037 waters: Geological Society of America Bulletin, v. 106, no. 11, p. 1430-1439.

1038 Surdam, R. C., and MacGowan, D. B., 1987, Oilfield waters and sandstone diagenesis: Applied
1039 Geochemistry, v. 2, no. 5-6, p. 613-619.

1040 Sverjensky, D. A., 1987, The role of migrating oil field brines in the formation of sediment-hosted Cu-
1041 rich deposits: Economic Geology, v. 82, no. 5, p. 1130-1141.

1042 Thackston J. W., McCulley B. L., and Preslo, L. M., 1981, Ground-water circulation in the western
1043 Paradox Basin, Utah: *in* Wiegand, D. L., ed., Geology of the Paradox basin: Rocky Mountain
1044 Association of Geologists Field Conference, p. 201-225

1045 Thamm, J. K., 1981, Geology and Recognition Criteria for Sandstone Uranium Deposits of the Salt Wash
1046 Type, Colorado Plateau Province: U.S. Department of Energy Open-File Report, no. GJBX-
1047 6(81).

1048 Thorson J. P., 2018, Paradox Basin fluids and Colorado Plateau copper, uranium, and vanadium deposits:
1049 Overview: Society of Economic Geologists, Guidebook Series, v. 59, p. 13-46.

1050 Thorson, J. P., and MacIntyre, T. J., 2005, Geology of the Cashin Mine sandstone-hosted disseminated
1051 copper deposit, Montrose County, Colorado: Society of Economic Geologists, Guidebook series,
1052 v. 37, p. 43-49.

Trudgill, B. D., 2011, Evolution of salt structures in the northern Paradox Basin: Controls on evaporite deposition, salt wall growth and supra-salt stratigraphic architecture: Basin Research, v. 23, no. 2, p. 208-238.

Turner-Peterson C. E., Santos E. S., and Fishman N. S., 1986, A basin analysis case study: The Morrison Formation Grants Uranium Region, New Mexico: American Association of Petroleum Geologists Studies in Geology, v. 22, p. 47-72.

Tuttle, M. L., Klett, T. R., Richardson, M., and Breit, G. N., 1996, Geochemistry of two interbeds in the Pennsylvanian Paradox Formation, Utah and Colorado: a record of deposition and diagenesis of repetitive cycles in a marine basin: U.S. Geological Survey Bulletin, no. 2000-N, 86 p.

Villegas M. E., Bachu S., Ramon J. C., and Underschultz J. R., 1994, Flow of Formation Waters in the Cretaceous—Miocene Succession of the Llanos Basin, Colombia: American Association of Petroleum Geologists Bulletin, v. 78, no. 12, p. 1843-1862.

Walker T. R., 1989, Application of diagenetic alterations in redbeds to the origin of copper in stratiform copper deposits, *in* Boyle, R.W., Brown, A.C., Jefferson, C.W., Jowett, E.C. and Kirkham, R.V. eds., Sediment-hosted stratiform copper deposits: Geological Association of Canada, Special Paper, v. 36, p. 85-96.

Waters, A. C., Wiesnet, D. R., Fleischer, M., Brant, R. A., Mapel, W. J., Granger, H. C., ... and Jones, B. E., 1949, Volcanic debris in uraniferous sandstones and its possible bearing on the origin and precipitation of uranium: US Department of the Interior, Geological Survey, no. 224-228.Whidden K. J., Lillis P. G., Anna L. O., Pearson K. M., and Dubiel R. F., 2014, Geology and total petroleum systems of the Paradox Basin, Utah, Colorado, New Mexico, and Arizona: The Mountain Geologist, v. 51, no. 2, p.119-138.

Wigley M., Kampman N., Dubacq B., and Bickle, M., 2012, Fluid-mineral reactions and trace metal mobilization in an exhumed natural CO_2 reservoir, Green River, Utah: Geology, v. 40, no. 6, p. 555-558.

Williams-Stroud S., 1994, The evolution of an inland sea of marine origin to a non-marine saline lake - The Pennsylvanian Paradox salt, in Sedimentology and Geochemistry of Modern and Ancient Saline Lakes: Society of Sedimentary Geology [SEPM] Special Publication, 50, p. 293-306.

Wilson, T. P., and Long, D. T., 1993a, Geochemistry and isotope chemistry of CaNaCl brines in Silurian strata, Michigan Basin, USA: Applied Geochemistry, v. 8, no. 5, p. 507-524.

Wilson, T. P., and Long, D. T., 1993b, Geochemistry and isotope chemistry of Michigan Basin brines: Devonian formations: Applied Geochemistry, v. 8, no. 1, p. 81-100.

Woodward-Clyde Consultants, 1982, Geologic characterization report for the Paradox basin study region, Utah study areas: volume II, Gibson Dome: Battelle Memorial Institute, Office of Nuclear Waste Isolation, 290 p.

Woodward-Clyde Consultants, 1983, Overview of the regional geology of the Paradox Basin study region: Columbus, Ohio, Office of Nuclear Waste Isolation Technical Report ONWI-92, 433 p.

Zhu, C., Winterle, J. R., and Love, E. I., 2003, Late Pleistocene and Holocene groundwater recharge from the chloride mass balance method and chlorine-36 data: Water Resources Research, v. 39, no. 7.

1092 Zielinski R. A., Bloch S., and Walker T. R., 1983, The mobility and distribution of heavy metals during
1093 the formation of first cycle red beds: Economic Geology, v. 78, no. 8, p. 1574-15.

Figure 1. (a) Location and geological features of the Paradox Basin, modified from Barton et al. (2018). Dashed line represents the basin extent. Location of water sampling points are showing in the blue star symbol. Iconic manifestations of paleofluid flow in the Paradox Basin are represented in color areas on the map. (b) Schematic cross section of A - A' in (a) across the Paradox Basin at late Middle Pennsylvanian time, modified from Whidden et al. (2014); Stevenson and Baars (1986). Extensive evaporite and interbedded black shales comprised the Pennsylvanian Paradox Formation in the northeastern part of basin. Algal bioherm mounds and shelf carbonates formed the southwestern part of the basin at late Middle Pennsylvanian time. (c) Schematic cross section of the northeastern part of the basin (B - B' in (a)) at present, modified from Baars (1966), Stevenson and Baars (1986), and King et al. (2014). Salt anticline structures and related fault systems are represented. Present hydrostratigraphy is divided into three (upper, middle, and lower) units.

Figure 2. Stratigraphic column of Devonian through Cretaceous formations with lithology, mineralization, and bleaching information in the Paradox Basin. Formations where water samples were collected from are identified in the black star symbol. Abbreviations used: Gp – Group; Ss – Sandstone; Fm – Formation; Mb – Member; Ls - Limestone.

Figure 3. Major cations (Na, Ca, Mg and K) versus Br concentrations of Paradox Basin formation waters, compared to the evaporated modern seawater line (McCaffrey et al., 1987). Major cations of salt anticline brine and Leadville Ls brines are enriched by dissolution of evaporites (e.g., halite, calcite, gypsum, and K-bearing evaporites). Honaker Trail Fm brines and Desert Creek brines show depleted K and Mg by formation of potassium aluminosilicates and dolomitization, and enriched Ca by albitization of plagioclase. Asterisk symbols represent data from previous literature: Salt anticline brine – Kharaka et al. (1997) and Rosenbauer et al. (1992); Groundwater in the Cutler Fm – Spangler et al. (1996); Paradox Fm brines and Leadville Ls brines – Blondes et al. (2018). Abbreviations used: Fm – Formation; Ls – Limestone; Ss – Sandstone.

Figure 4. (a) Na/Br versus Cl/Br ratios of formation waters to separate water types and origin of salinity. Based on modern seawater (Riley and Chester, 1971), the Salt Creek, Dolores River, salt anticline brine, and Leadville Ls brines show high Na/Br and Cl/Br ratios, while Honaker Trail Fm brines, Desert Creek brines, and Cane Creek brine exhibit low ratios. (b) Br versus Cl concentrations of formation waters. The salt anticline brine and Leadville Ls brines plot in the halite saturation zone. The Cane Creek brine shows the highest Br and Cl concentrations in this study and represents evaporated paleo-seawater. Asterisk symbols represent data from previous literature, as described in Fig. 2. Abbreviations used: Fm – Formation; Ls – Limestone; Ss – Sandstone.

Figure 5. Water stable isotopes of Paradox Basin formation waters compared to the global meteoric water line (GMWL; Craig, 1961) and local meteoric water line (LMWL) of Utah (Kendall and Coplen, 2001). Shallow groundwaters in the Burro Canyon Fm and Navajo Ss, salt anticline brine, Salt Creek, Dolores River, and Leadville Ls brines plot along the LMWL. Deep brines (Honaker Trail Fm, Desert Creek, Cane Creek, and McCracken Ss brines) and fluid inclusions in the Paradox Fm evaporites (Petrychenko et al., 2012) plot below the LMWL. The Honaker Trail Fm and Desert Creek brines show mixing trends between evaporated paleo-seawater (EPS; endmember 1 (EM1)) and meteoric water (EM2). Asterisk symbols represent data from previous literature:

Groundwater in the Cutler Fm – Spangler et al. (1996); Paradox Fm brines – Spangler et al. (1996) and Naftz et al. (1997); Leadville Ls brines – Nuckolls and McCulley (1987). Abbreviations used: Fm – Formation; Ls – Limestone; Ss – Sandstone; EM – Endmember.

Figure 6. (a) Sulfur and oxygen isotopes of SO_4 and (b) sulfur isotopes of SO_4 versus SO_4 concentrations of Paradox Basin formation waters to distinguish sources of SO_4. Evaporite (anhydrite) data in the Paradox Fm are from Chen et al. (2016) and Holt et al. (2014). Sulfate in most of the basinal brine samples came from dissolution of evaporites. Honaker Trail Fm brines, groundwater in the Burro Canyon Fm, and Dolores River have another SO_4 sourced from sulfide oxidation. Enrichment factors of sulfur isotopes of sulfate and H_2S for salt anticline brine and Salt Creek indicate bacterial sulfate reduction. Abbreviations used: Fm – Formation; Ls – Limestone; Ss – Sandstone.

Figure 7. Sr isotopes ratios and concentrations (mmol/L) of Paradox Basin formation waters. Leadville Ls brine and McCracken Ss brines have high Sr isotopes ratios, consistent with endogenic springs in the Grand Canyon region in the Colorado Plateau ([1] Crossey et al., 2006). Sr isotope ratios and concentrations of groundwater in Burro Canyon Fm and Navajo Ss are similar with those of hematite and calcite in the Jurassic Ss ([2] Chan et al., 2000). Sr isotopes of Cane Creek and Desert Creek brines are consistent with those of anhydrite in the Pennsylvanian Hermosa Fm (Paradox Fm and/or Honaker Trail Fm; [3] Breit et al., 1990). Sr isotope data of barite in the Hermosa and Morrison formations are from [3] Breit et al. (1990). Asterisk and x symbols represent data from previous literature (Spangler et al., 1996 and Naftz et al., 1997). Abbreviations used: Fm – Formation; Ls – Limestone; Ss – Sandstone. The solid and dotted black lines are mixing lines between the salt anticline brines and the Dolores River and Navajo Ss waters with the highest $^{87}Sr/^{86}Sr$.

Figure 8. Concentration of Cu, U, Fe and Mn versus dissolved H_2S in various formation waters. Note that U concentration is in nmol/L and other metals are in μmol/L, while dissolved H_2S is in mmol/L. H_2S concentrations of groundwater in the Burro Canyon Fm and Navajo Ss are assumed to be negligible. Groundwater in the Burro Canyon Fm exhibits the highest U concentration in this study. The Honaker Trail Fm and Cane Creek brines show the highest Cu, Fe, and Mn concentrations in presence of high H_2S. The Desert Creek brines contain varied H_2S concentrations and low Cu and U concentration below detection limit. The salt anticline brine shows high H_2S because of bacterial sulfate reduction and moderate Cu, Fe and Mn concentrations. Metal concentrations of groundwater in the Morrison Fm came from Phoenix (1959). Abbreviations used: Fm – Formation; Ls – Limestone; Ss – Sandstone.

Figure 9. Conceptual model of the types, sources, and distributions of distinct compositions of formation waters and water-rock reactions in the Paradox Basin today. Orange arrows represent local topographic recharge and meteoric influx into upper (including Burro Canyon Fm, Navajo Ss, and Honaker Trail Fm) and lower (including Leadville Ls and McCracken Ss) hydrostratigraphic units. Abbreviations used: Fm – Formation; Ls – Limestone; Ss – Sandstone; EPS – Evaporated Paleo-Seawater.

Figure 1

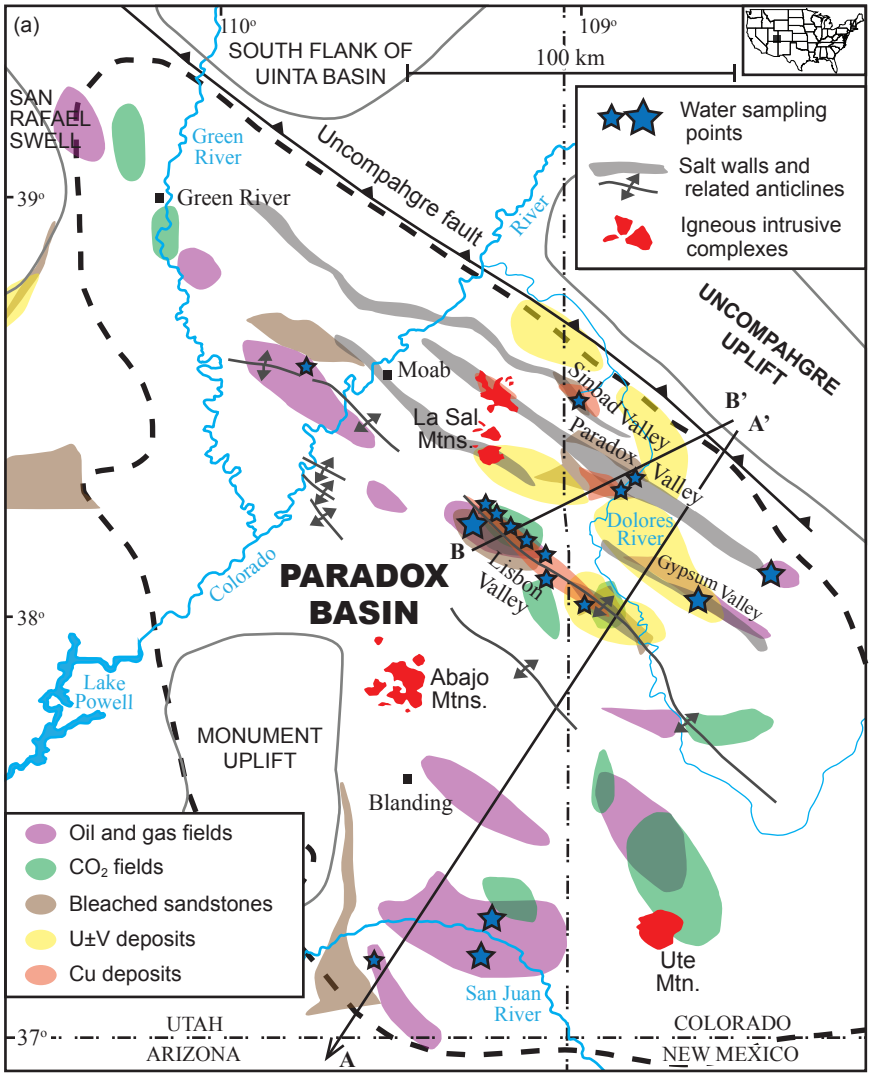

(b) Schematic cross section across Paradox Basin at late Middle Pennsylvanian time

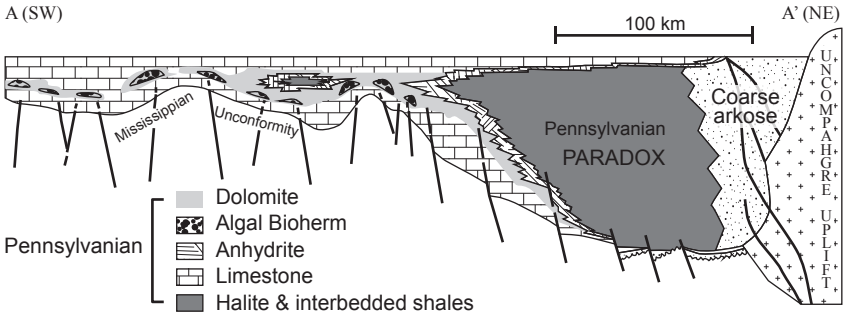

(c) Schematic cross section across Northeastern Paradox Basin Today

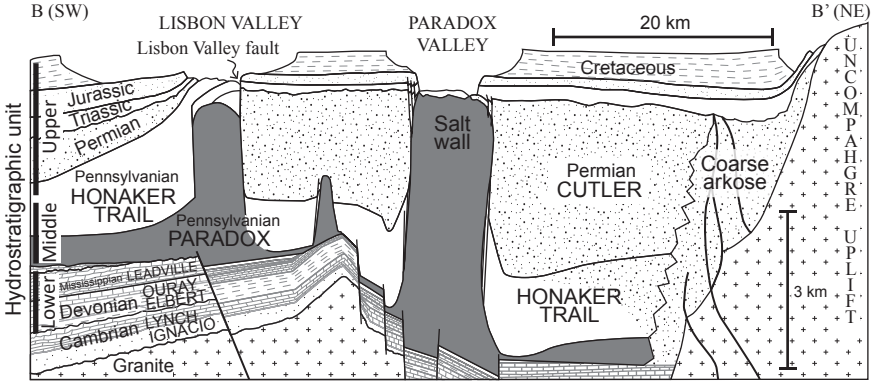

Figure 2

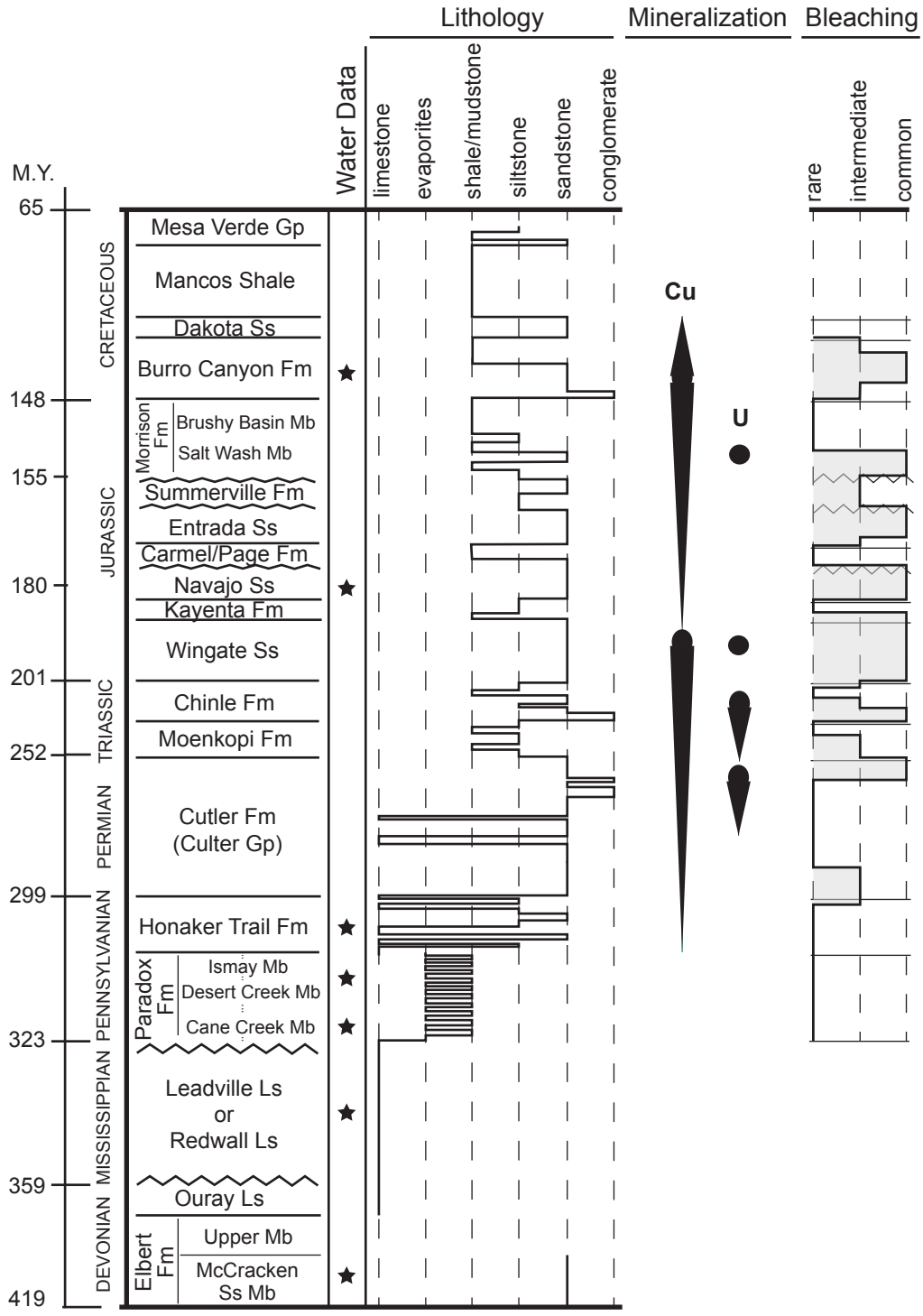
Lithology
Mineralization
Bleaching
Water Data
limestone
evaporites
shale/mudstone
siltstone
sandstone
conglomerate
rare
intermediate
common
M.Y.
65
148
155
180
201
252
299
323
359
419
CRETACEOUS
JURASSIC
TRIASSIC
PERMIAN
PENNSYLVANIAN
MISSISSIPPIAN
DEVONIAN
Mesa Verde Gp
Mancos Shale
Dakota Ss
Burro Canyon Fm
Morrison Fm
Brushy Basin Mb
Salt Wash Mb
Summerville Fm
Entrada Ss
Carmel/Page Fm
Navajo Ss
Kayenta Fm
Wingate Ss
Chinle Fm
Moenkopi Fm
Cutler Fm
(Culter Gp)
Honaker Trail Fm
Paradox Fm
Ismay Mb
Desert Creek Mb
Cane Creek Mb
Leadville Ls
or
Redwall Ls
Ouray Ls
Elbert Fm
Upper Mb
McCracken
Ss Mb
Cu
U

Figure 3

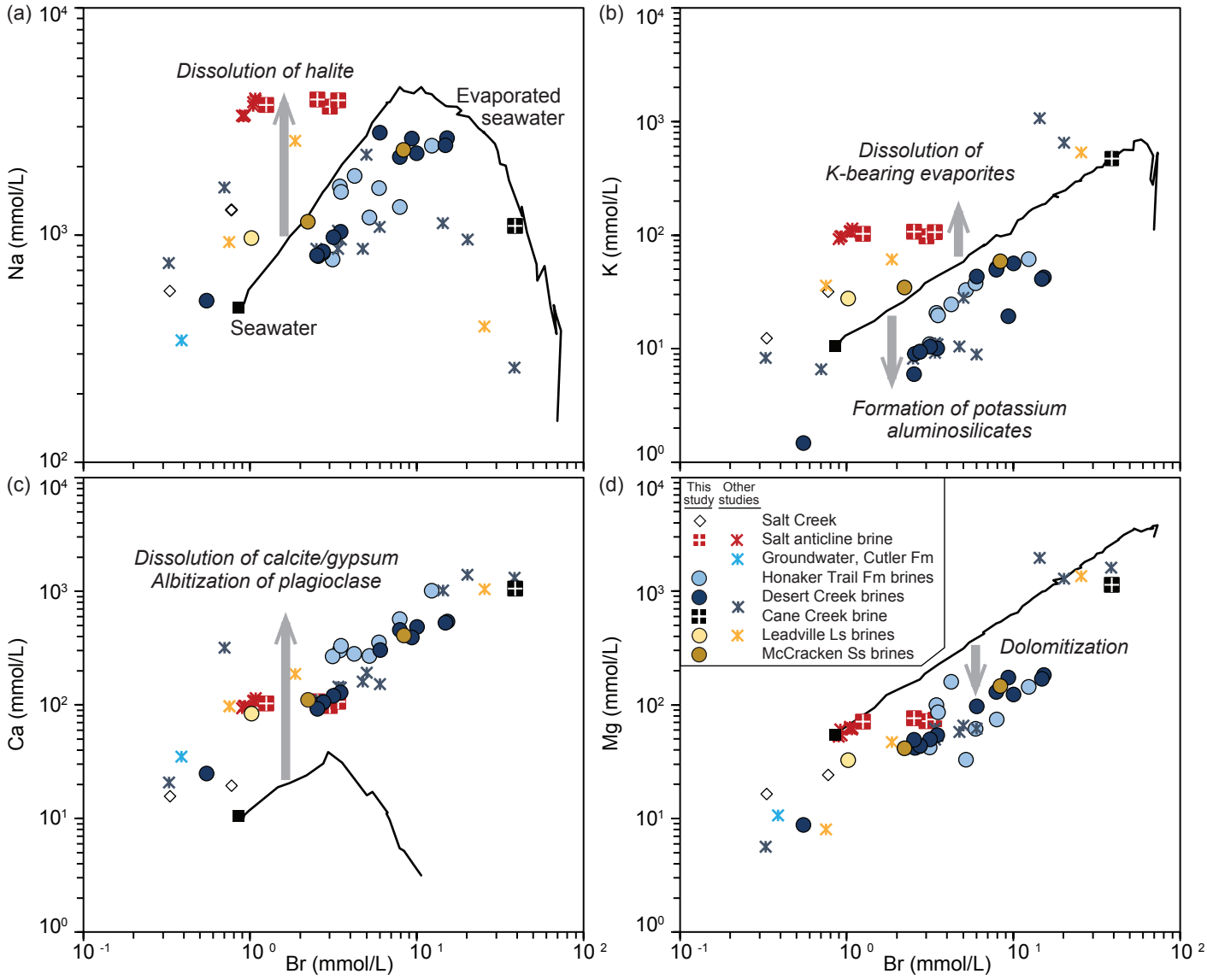
(a)
Na (mmol/L)
Dissolution of halite
Evaporated seawater
Seawater
(b)
K (mmol/L)
Dissolution of K-bearing evaporites
Formation of potassium aluminosilicates
(c)
Ca (mmol/L)
Dissolution of calcite/gypsum
Albitization of plagioclase
Br (mmol/L)
(d)
Mg (mmol/L)
Dolomitization
Br (mmol/L)
This study
Other studies
Salt Creek
Salt anticline brine
Groundwater, Cutler Fm
Honaker Trail Fm brines
Desert Creek brines
Cane Creek brine
Leadville Ls brines
McCracken Ss brines

Figure 4

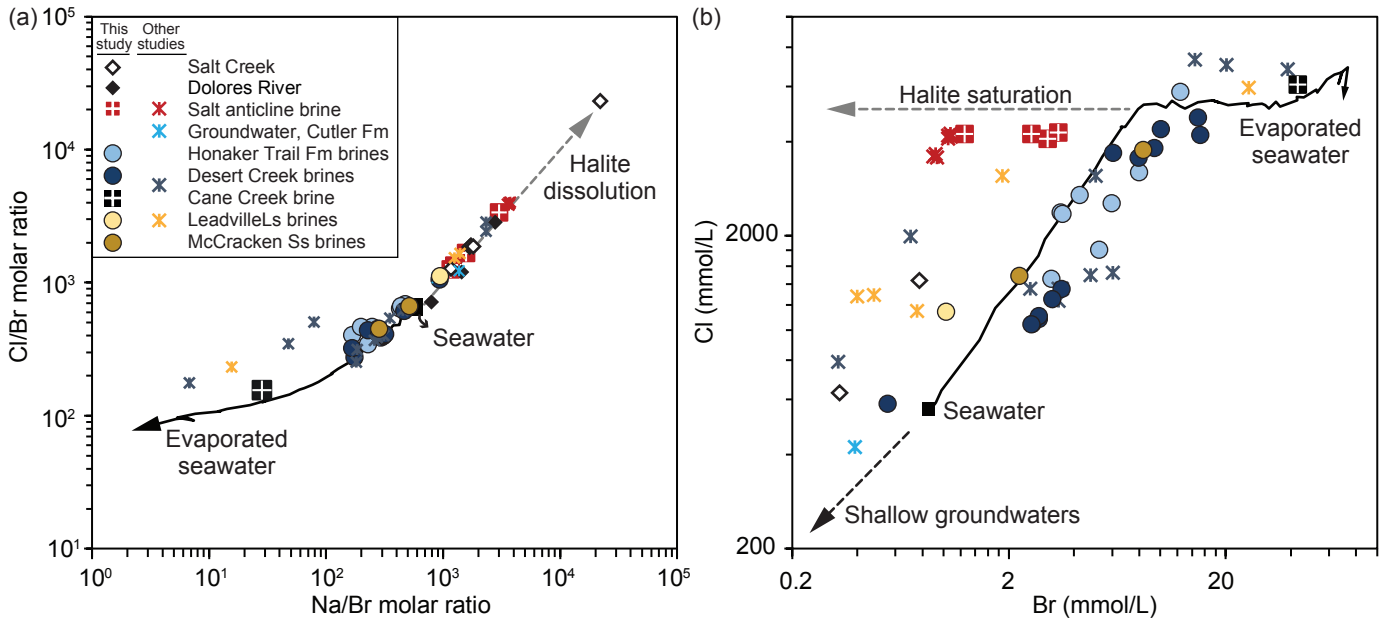
(a)
This study
Other studies
Salt Creek
Dolores River
Salt anticline brine
Groundwater, Cutler Fm
Honaker Trail Fm brines
Desert Creek brines
Cane Creek brine
LeadvilleLs brines
McCracken Ss brines
Halite dissolution
Seawater
Evaporated seawater
Cl/Br molar ratio
Na/Br molar ratio
(b)
Halite saturation
Evaporated seawater
Seawater
Shallow groundwaters
Cl (mmol/L)
Br (mmol/L)

Figure 5

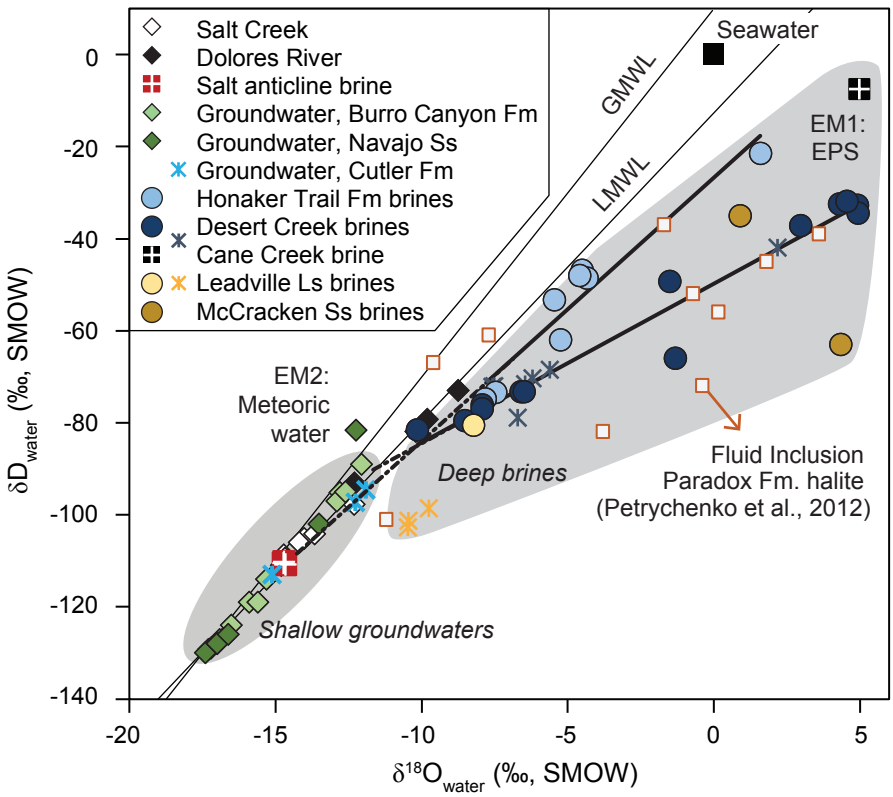
Salt Creek
Dolores River
Salt anticline brine
Groundwater, Burro Canyon Fm
Groundwater, Navajo Ss
Groundwater, Cutler Fm
Honaker Trail Fm brines
Desert Creek brines
Cane Creek brine
Leadville Ls brines
McCracken Ss brines
Seawater
GMWL
LMWL
EM1:
EPS
EM2:
Meteoric
water
Deep brines
Fluid Inclusion
Paradox Fm. halite
(Petrychenko et al., 2012)
Shallow groundwaters
0
-20
-40
-60
-80
-100
-120
-140
-20
-15
-10
-5
0
5
δD water (‰, SMOW)
δ18O water (‰, SMOW)

Figure 6

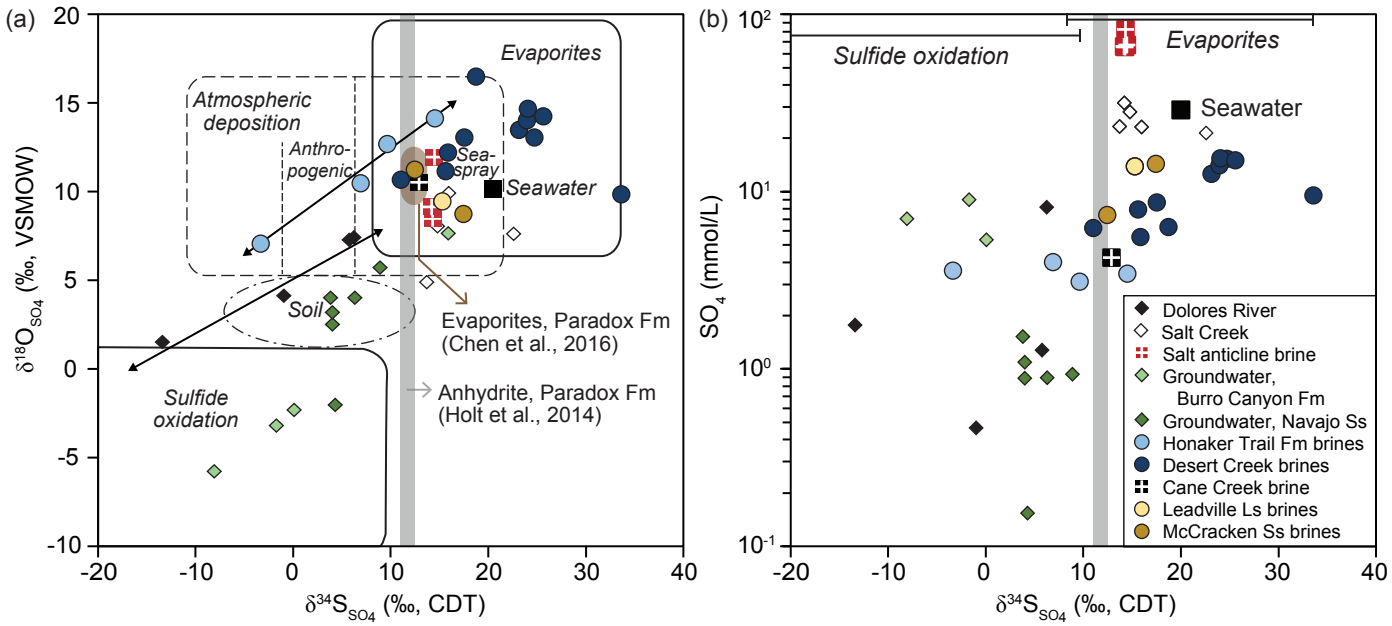
(a)
Evaporites
Atmospheric deposition
Anthro-pogenic
Sea-spray
Seawater
Soil
Sulfide oxidation
Evaporites, Paradox Fm (Chen et al., 2016)
Anhydrite, Paradox Fm (Holt et al., 2014)
δ18OSO4 (‰, VSMOW)
δ34SSO4 (‰, CDT)
(b)
Sulfide oxidation
Evaporites
Seawater
SO4 (mmol/L)
δ34SSO4 (‰, CDT)
Dolores River
Salt Creek
Salt anticline brine
Groundwater, Burro Canyon Fm
Groundwater, Navajo Ss
Honaker Trail Fm brines
Desert Creek brines
Cane Creek brine
Leadville Ls brines
McCracken Ss brines

Figure 7

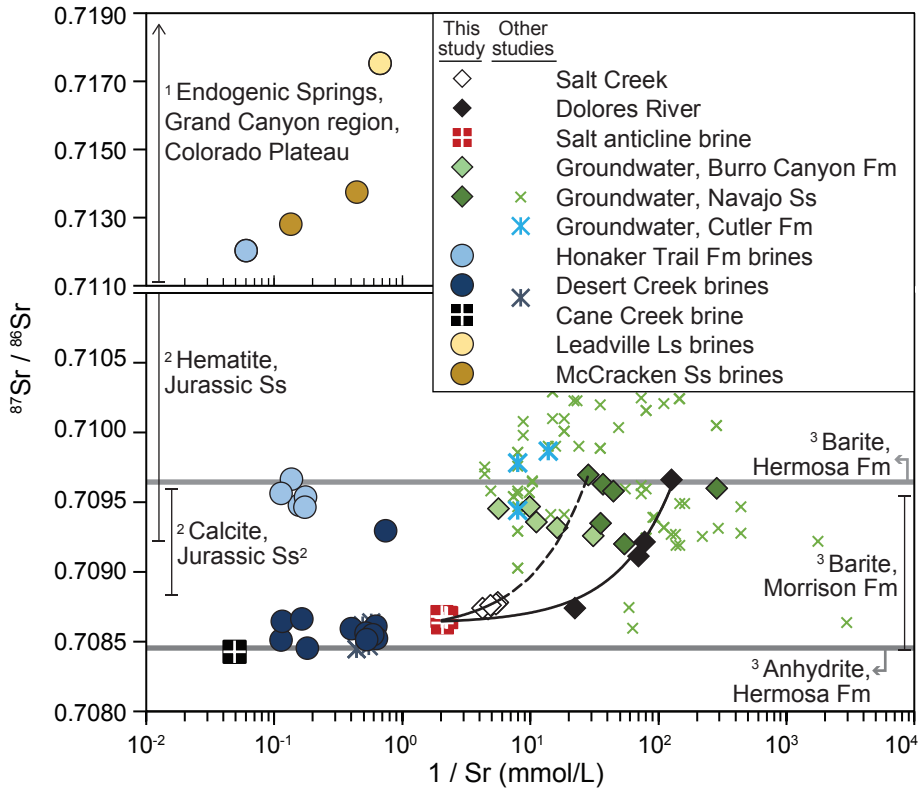
0.7190
0.7170
0.7150
0.7130
0.7110
0.7105
0.7100
0.7095
0.7090
0.7085
0.7080
87Sr / 86Sr
10-2
10-1
100
101
102
103
104
1 / Sr (mmol/L)
This study
Other studies
Salt Creek
Dolores River
Salt anticline brine
Groundwater, Burro Canyon Fm
Groundwater, Navajo Ss
Groundwater, Cutler Fm
Honaker Trail Fm brines
Desert Creek brines
Cane Creek brine
Leadville Ls brines
McCracken Ss brines
1 Endogenic Springs, Grand Canyon region, Colorado Plateau
2 Hematite, Jurassic Ss
2 Calcite, Jurassic Ss2
3 Barite, Hermosa Fm
3 Barite, Morrison Fm
3 Anhydrite, Hermosa Fm

Figure 8

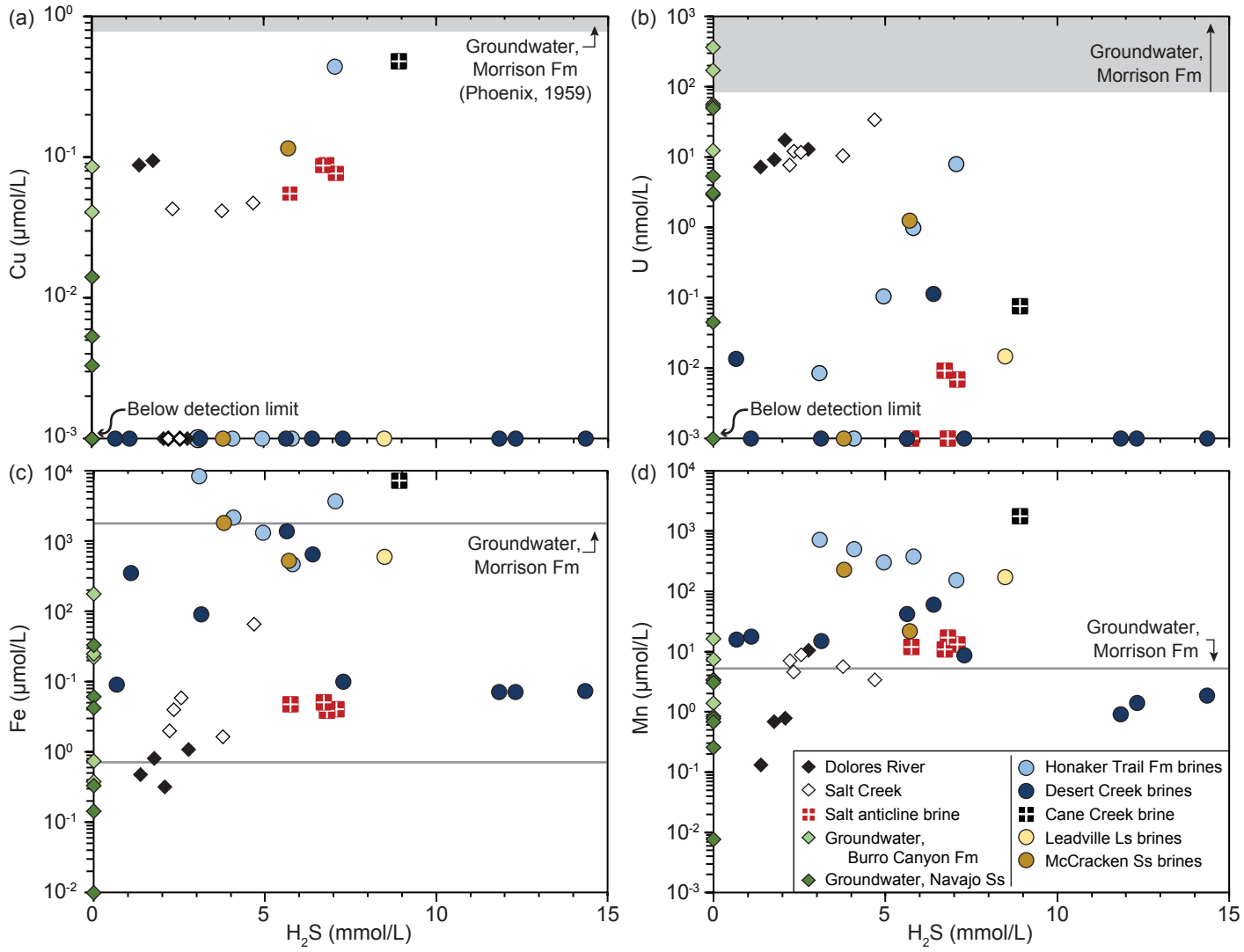
(a)
Cu (µmol/L)
Groundwater, Morrison Fm (Phoenix, 1959)
Below detection limit
(b)
U (nmol/L)
Groundwater, Morrison Fm
Below detection limit
(c)
Fe (µmol/L)
Groundwater, Morrison Fm
H2S (mmol/L)
(d)
Mn (µmol/L)
Groundwater, Morrison Fm
H2S (mmol/L)
Dolores River
Salt Creek
Salt anticline brine
Groundwater, Burro Canyon Fm
Groundwater, Navajo Ss
Honaker Trail Fm brines
Desert Creek brines
Cane Creek brine
Leadville Ls brines
McCracken Ss brines

Figure 9

Honaker Trail Fm brines

- EPS-derived brine mixed with meteoric water
- Oxidation of Sulfides
- Hydrocarbon-bearing reducing fluid with high H_2S

Fresh-brackish groundwater in Burro Canyon Fm/Navajo Ss

- Sulfide oxidation by influx of meteoric water
- High U content

Salt anticline brine

- Topographically-driven meteoric dissolution of evaporites around salt anticlines (Na-Cl type brine)
- High H_2S from bacterial sulfate reduction

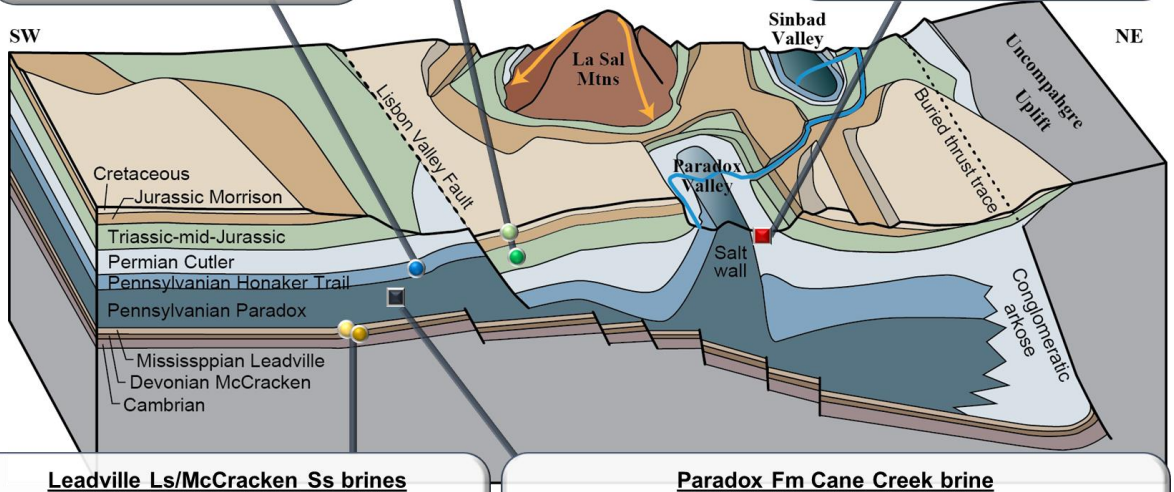

Leadville Ls/McCracken Ss brines

- Salt dissolution-derived brine by influx of meteoric water
- Radiogenic Sr from interaction with basement rocks or shales in basal sediments

Paradox Fm Cane Creek brine

- Highly evaporated paleo-seawater (EPS) associated with Paradox Formation (Ca-Cl type brine)
- Hydrocarbon-bearing reducing fluid with high H_2S
- One type of fluid responsible for sandstone bleaching

TABLE 1. LOCATION AND FIELD MEASUREMENT OF WATER SAMPLES

Sample/Well ID	Latitude	Longitude	Elevation m	Field	Formation	Depth m	pH -	Temp. ℃	E.C. mS/cm	Alkalinity meq/L	Density g/cm^3
Surface water and seeps											
DR-BR-a	38.30997	-108.88583	1500	Paradox Valley	-	0	7.68	6.9	0.8	2.62	0.9980
DR-BR-b	38.30997	-108.88583	1500	Paradox Valley	-	0	8.23	24.3	1.6	3.57	1.0011
DR North-a	38.34943	-108.85152	1495	Paradox Valley	-	0	8.10	8.05	4.4	2.93	0.9996
DR-North-b	38.34943	-108.85152	1495	Paradox Valley	-	0	8.07	29.1	26.2	5.19	1.0123
Salt Creek 1a	38.52593	-108.98061	1629	Sinbad Valley	-	0	7.35	12.6	65.0	4.44	1.0280
Salt Creek 1b	38.52593	-108.98061	1629	Sinbad Valley	-	0	7.75	22.5	118.0	3.99	1.0635
Salt Creek 2	38.51950	-108.98237	1634	Sinbad Valley	-	0	7.05	10.9	129.8	5.07	1.0042
Salt Creek Seep1	38.52593	-108.98061	1629	Sinbad Valley	-	0	7.65	7.1	123.0	5.25	1.0604
Salt Creek Seep2	38.51991	-108.98160	-	Sinbad Valley	-	0	7.52	30.3	18.8	5.51	1.0101
Groundwater monitoring wells											
PW-3a	38.14729	-109.13597	1948	Lisbon Valley	K. Burro Canyon Fm	148	6.69	16	1.7	6.75	-
PW-3b	38.14729	-109.13584	1938	Lisbon Valley	K. Burro Canyon Fm	145	7.31	17	1.7	6.99	1.0014
PW-4	38.15272	-109.14219	1929	Lisbon Valley	K. Burro Canyon Fm	130	6.75	14.7	2.0	6.12	1.0018
PW-12a	38.1249	-109.12121	1969	Lisbon Valley	K. Burro Canyon Fm	305	7.1	20.7	1.5	6.28	-
PW-12b	38.12460	-109.12093	2001	Lisbon Valley	K. Burro Canyon Fm	305	7.35	20	1.5	6.32	1.0013
325	38.12001	-109.10598	1941	Lisbon Valley	K. Burro Canyon Fm	159	7.14	20.8	1.2	-	-
MW96-7A	38.14576	-109.13056	1966	Lisbon Valley	K. Burro Canyon Fm	364	8.27	13.5	2.0	6.29	-
98R7	38.15165	-109.14013	1940	Lisbon Valley	K. Burro Canyon Fm	102	7.86	11.1	0.9	-	-
98R4	38.15541	-109.14478	1938	Lisbon Valley	K. Burro Canyon Fm	139	7.72	17.1	1.1	-	-
PW-1	38.151	-109.13995	1941	Lisbon Valley	K. Burro Canyon Fm	110	7.06	15.5	1.1	-	-
PW-2	38.15148	-109.13867	1950	Lisbon Valley	K. Burro Canyon Fm	229	6.87	15.9	1.9	-	-
PW-7a	38.12497	-109.11137	1929	Lisbon Valley	J. Navajo Ss	457	7.73	24.3	0.6	4.13	1.0006
PW-7b	38.12493	-109.11143	1943	Lisbon Valley	J. Navajo Ss	463	6.8	24.1	0.6	-	-
PW-8a	38.14782	-109.13432	1954	Lisbon Valley	J. Navajo Ss	474	7.49	24.8	1.1	6.41	-
PW-8b	38.14783	-109.13448	1946	Lisbon Valley	J. Navajo Ss	472	7.99	24.5	1.2	6.40	1.0008
PW-11a	38.12608	-109.10066	1930	Lisbon Valley	J. Navajo Ss	457	7.77	24.4	0.9	4.14	-
PW-11b	38.12621	-109.10073	1926	Lisbon Valley	J. Navajo Ss	457	7.68	24.8	0.9	4.63	1.0006
LV-41-75	38.11587	-109.11999	2026	Lisbon Valley	J. Navajo Ss	176	6.93	20.3	0.4	-	-
MW97-11	38.13831	-109.13161	2014	Lisbon Valley	J. Navajo Ss	338	7.95	19.6	0.9	-	-
MW97-13	38.12695	-109.10746	1950	Lisbon Valley	J. Navajo Ss	439	6.99	18.8	0.6	-	-
MW06-15	38.15727	-109.1401	1941	Lisbon Valley	J. Navajo Ss	274	8.77	17.6	1.3	-	-
Brine pumping wells											
BOR well 2E	38.32630	-108.86042	1501	Paradox Valley	Salt anticline	14	6.41	16	235.4	4.79	1.1678
BOR well 3E	38.32697	-108.85925	1503	Paradox Valley	Salt anticline	14	6.46	18	235.2	4.93	1.1677
BOR well 8E	38.34356	-108.85565	1486	Paradox Valley	Salt anticline	14	6.53	15.6	234.8	4.52	1.1670
BOR well 9E	38.34318	-108.85670	1491	Paradox Valley	Salt anticline	14	6.56	15.1	232.7	4.50	1.1620

Oil/gas producing wells											
MM 31-42	38.23187	-109.20990	2062	Lisbon Valley	pC. Honaker Trail Fm	1617	6.40	-	-	0.64	1.0605
MM 31-31	38.23625	-109.21529	-	Lisbon Valley	pC. Honaker Trail Fm	1522	5.66	-	168.5	4.74	1.1174
MM 5-6	38.22772	-109.20319	-	Lisbon Valley	pC. Honaker Trail Fm	1618	5.58	-	206.5	1.55	1.2076
HC 12-13	38.09464	-108.46845	2159	Lisbon Valley	pC. Honaker Trail Fm	2280	6.46	17.8	4.0	1.70	1.0746
FF-5	38.06332	-108.68227	2022	Lisbon Valley	pC. Honaker Trail Fm	2510	6.46	15.8	110.3	1.71	1.1014
Big Indian 24-31	38.16899	-109.13400	1920	Lisbon Valley	pC. Honaker Trail Fm	947	6.26	23.5	-	5.42	1.1060
BH 10-31	38.19219	-109.17191	2071	Lisbon Valley	pC. Honaker Trail Fm	1184	6.28	15.8	139.2	1.20	1.0948
BH 10-42	38.18850	-109.16347	-	Lisbon Valley	P. Culter Fm – Ps. Honaker Trail Fm	1090	6.15	22.5	64.8	2.83	1.0955
Anasazi 1	37.16669	-109.31075	1457	Greater Aneth oil field	Ps. Paradox Fm, Desert Creek member	1762	6.28	-	38.9	0.83	1.0248
Runway-10-E2	37.32613	-109.16508	1661	Greater Aneth oil field	Ps. Paradox Fm, Desert Creek member	1839	6.62	17.7	32.7	1.56	1.1481
Sahgzie 1a	37.16963	-109.30639	1446	Greater Aneth oil field	Ps. Paradox Fm, Desert Creek member	1954	6.02	25.4	-	2.54	1.1679
Sahgzie 1b	37.16963	-109.30639	1446	Greater Aneth oil field	Ps. Paradox Fm, Desert Creek member	1954	5.92	-	217.9	1.92	1.1709
Monument-8N-2a	37.31628	-109.19794	1664	Greater Aneth oil field	Ps..Paradox Fm, Desert Creek member	1895	5.78	30.5	-	5.68	1.1409
Monument-8N-2b	37.31628	-109.19794	1664	Greater Aneth oil field	Ps. Paradox Fm, Desert Creek member	1895	5.57	-	215.8	3.92	1.1589
WM 22-43	37.19517	-109.27129	-	Greater Aneth oil field*	Ps. Paradox Fm, Desert Creek member	1722	6.61	-	101.8	3.94	1.0587
WM 34-24	37.17509	-109.27126	1496	Greater Aneth oil field*	Ps. Paradox Fm, Desert Creek member	1722	6.19	-	91.7	7.97	1.0497
WM 34-31	37.18485	-109.26808	1447	Greater Aneth oil field*	Ps. Paradox Fm, Desert Creek member	1722	6.15	-	90.1	7.14	1.0499
WM 34-33	37.17855	-109.26788	1514	Greater Aneth oil field*	Ps. Paradox Fm, Desert Creek member	1722	6.22	-	87.1	7.91	1.0473
Injection water	37.18861	-109.27979	1408	Greater Aneth oil field*	Ps. Paradox Fm, Desert Creek member	1722	6.38	-	34.0	5.34	1.0555
TOHO 35-B	37.18559	-109.57544	1453	Greater Aneth oil field	Ps. Paradox Fm, Desert Creek member-Ismay member	-	6.75	28.7	209.1	1.97	1.1541
TOHO 1	37.17495	-109.57433	1445	Greater Aneth oil field	Ps. Paradox Fm, Desert Creek member-Ismay member	-	7.25	-	87.6	12.55	1.0474
McIntyre 17-21	38.07719	-108.99125	1903	Lisbon Valley	M. Leadville Ls	2586	6.78	14.2	58.5	12.28	1.0487
Lisbon 10-33	38.19150	-109.27369	1972	Lisbon Valley	D. McCracken Ss	2702	5.62	14.9	-	1.82	1.1427
Lisbon B8-10	38.19008	-109.27585	1950	Lisbon Valley	D. McCracken Ss	2610	7.05	17.8	0.0	11.36	1.0616
Lithium exploratory well											
Cane Creek 32	38.58033	-109.73555	1586	NW of Moab	Ps. Paradox Fm, Cane Creek member	-	5.18	34.8	168.5	0.00	1.2704

* Water injection activity

Note: In Formation column, abbreviations of geological period indicate K (Cretaceous), J (Jurassic), P (Permian), Ps (Pennsylvanian), M (Mississippian), and D (Devonian).

TABLE 2. CHEMICAL DATA FROM WATER SAMPLES COLLECTED IN THE STUDY AREA

Sample/Well ID	T.D.S. g/L	Cl mmol/L	Br mmol/L	SO_4 mmol/L	Ca mmol/L	Mg mmol/L	Na mmol/L	K mmol/L	Sr mmol/L	Si mmol/L	H_2S mmol/L	Ba µmol/L	Mn µmol/L	Fe µmol/L	Cu µmol/L	U nmol/L
Surface water and seeps																
DR-BR-a	0.47	3.2	0.004	0.5	1.2	0.5	3.5	0.1	0.01	0.08	1.4	1.1	0.1	0.5	0.09	7
DR-BR-b	1.00	7.7	0.006	1.8	2.2	1.0	9.2	0.3	0.01	0.10	2.1	1.8	0.8	0.3	bdl*	17
DR North-a	2.24	31	0.011	1.3	1.6	1.3	30	0.7	0.01	0.09	1.8	1.0	0.7	0.8	0.09	9
DR-North-b	17	261	bdl	8.2	5.3	7.2	238	6.6	0.04	0.05	2.8	3.1	11	1.1	bdl	13
Salt Creek 1a	39	629	0.330	23.4	15.7	16.5	567	12.4	0.18	0.21	2.3	0.4	4.6	4.0	0.04	12
Salt Creek 1b	87	1411	0.061	31.7	22.5	26.3	1327	31.3	0.24	bdl	2.2	1.3	7.1	2.0	bdl	8
Salt Creek 2	7.23	70	0.055	21.5	14.4	10.9	64	1.0	0.19	0.24	4.7	0.3	3.4	66	0.05	34
Salt Creek Seep1	86	1437	0.772	28.2	19.4	24.2	1290	31.9	0.22	0.30	3.8	0.3	5.7	1.7	0.04	10
Salt Creek Seep2	12	148	0.079	23.2	18.0	14.8	142	2.5	0.21	0.25	2.6	0.5	8.9	5.9	bdl	12
Groundwater monitoring wells																
PW-3a	1.51	0.5	0.004	7.0	5.6	3.4	2.8	0.3	0.16	0.21	na†	na	na	na	na	na
PW-3b	1.49	0.5	0.006	6.7	5.6	3.2	2.7	0.3	0.18	0.17	na	0.1	3.4	22	bdl	172
PW-4	1.91	0.4	0.006	10.3	9.2	3.7	2.0	0.2	0.10	0.16	na	0.1	16	177	bdl	363
PW-12a	1.27	0.5	0.005	5.4	3.3	1.9	6.8	0.3	0.06	0.24	na	na	na	na	na	na
PW-12b	1.26	0.5	0.007	5.1	3.1	2.0	7.8	0.2	0.06	0.18	na	0.1	7.5	25	bdl	56
325	1.21	0.9	0.005	0.8	1.0	0.8	12	0.3	0.03	0.14	na	0.6	1.4	0.4	0.09	53
MW96-7A	1.73	0.6	0.004	9.0	5.7	4.0	4.9	0.3	0.09	0.16	na	0.1	0.8	0.7	0.04	12
PW-7a	0.54	1.1	0.005	0.8	1.1	0.6	4.0	0.1	0.03	0.24	na	0.3	0.7	6.1	bdl	3
PW-7b	0.60	2.1	0.005	0.9	1.0	0.7	4.4	0.2	0.03	0.23	na	na	na	na	na	na
PW-8a	0.89	3.4	0.003	1.1	0.6	0.7	9.4	0.3	0.02	0.33	na	na	na	na	na	na
PW-8b	0.88	3.3	0.006	1.1	0.6	0.7	9.2	0.2	0.02	0.17	na	0.3	0.3	bdl	bdl	0.05
PW-11a	0.67	3.4	0.005	0.9	1.1	0.8	5.3	0.2	0.03	0.28	na	na	na	na	na	na
PW-11b	0.70	3.4	0.008	0.9	1.1	0.8	5.6	0.2	0.04	0.22	na	0.3	0.8	33	bdl	bdl
LV-41-75	0.34	0.5	0.005	0.2	1.3	0.7	0.5	0.0	0.004	0.22	na	2.1	0.0	0.1	0.01	5
MW97-11	0.90	3.0	0.004	1.5	1.7	1.0	6.3	0.2	0.03	0.25	na	0.3	3.3	0.3	0.01	50
MW97-13	0.54	1.3	0.004	0.9	1.2	0.7	3.1	0.2	0.02	0.25	na	2.9	3.1	4.2	0.003	3
Brine pumping wells																
BOR well 2E	256	4269	3.379	66.2	36.0	74.5	3915	107	0.46	bdl	6.7	0.4	11	5.1	0.09	0.01
BOR well 3E	255	4234	2.538	65.8	36.6	76.5	3952	107	0.49	bdl	6.8	0.5	17	3.9	0.09	bdl
BOR well 8E	250	4230	1.250	67.6	35.0	71.6	3735	103	0.45	bdl	7.1	0.3	13	4.1	0.08	0.01
BOR well 9E	245	4083	3.012	82.7	37.3	71.6	3676	98	0.49	bdl	5.8	0.4	12	4.8	0.06	bdl
Oil/gas producing wells																
MM 31-42	83	1456	3.146	5.9	264	42	779	11	5.70	bdl	na	7.9	344	147	0.12	0.01
MM 31-31	171	3188	7.959	2.4	561	74	1327	51	na	na	na	na	na	na	na	na
MM 5-6	308	5755	12.36	1.7	1003	144	2466	61	na	na	na	na	na	na	na	na
HC 12-13	106	1798	5.222	4.0	268	33	1195	33	7.36	bdl	3.1	42	712	8277	bdl	0.01
FF-5	146	2534	5.949	3.6	353	61	1603	38	16	0.45	4.1	308	503	2150	bdl	bdl
Big Indian 24-31	155	2697	4.246	5.9	279	158	1816	25	5.72	0.47	7.1	161	153	3648	0.44	8

BH 10-31	136	2344	3.534	3.1	329	85	1549	20	8.80	bdl	5.8	1070	373	467	bdl	1
BH 10-42	138	2372	3.467	3.4	298	99	1636	21	6.37	bdl	5.0	357	299	1310	bdl	0.10
Anasazi 1	34	581	0.551	6.2	24	8.8	514	1.5	1.35	0.15	0.7	1.4	16	9.0	bdl	0.01
Runway-10-E2	213	3677	6.038	7.9	306	96	2817	43	6.06	bdl	3.1	1.9	15	90	bdl	bdl
Sahgzie 1a	240	4184	15.26	5.5	547	182	2671	42	8.83	bdl	na	4.0	18	349	bdl	bdl
Sahgzie 1b	255	4767	14.89	2.7	534	169	2475	41	na	na	na	na	na	na	na	na
Monument-8N-2a	202	3541	7.927	8.7	459	130	2198	50	8.60	bdl	5.6	5.3	42	1377	bdl	bdl
Monument-8N-2b	234	4372	10.04	5.9	489	123	2288	56	na	na	na	na	na	na	na	na
WM 22-43	80	1349	3.509	12.6	128	54	1031	10	2.49	0.19	7.3	1.1	8.7	9.9	bdl	bdl
WM 34-24	67	1106	2.755	15.0	105	43	846	9.4	1.69	0.25	14	0.9	1.9	7.3	bdl	bdl
WM 34-31	65	1082	2.745	15.3	104	43	833	9.4	1.60	0.23	12	0.5	0.9	7.1	bdl	bdl
WM 34-33	63	1043	2.569	15.4	99	42	805	9.0	1.58	0.25	12	0.6	1.4	7.1	bdl	bdl
Injection water	75	1251	3.174	14.1	120	49	978	10	1.92	0.24	na	2.8	3.4	14	bdl	bdl
TOHO 35-B	219	3812	9.361	6.3	395	173	2649	19	5.50	bdl	6.4	6.3	60	637	bdl	0.11
TOHO 1	63	1039	2.537	9.5	92	49	812	6.0	1.89	0.20	na	5.1	6.4	179	bdl	0.03
McIntyre 17-21	70	1143	1.025	13.9	83	33	968	28	1.48	0.61	8.5	2.5	169	589	bdl	0.01
Lisbon 10-33	212	3747	8.353	7.4	410	146	2363	59	7.42	bdl	3.8	27	228	1786	bdl	bdl
Lisbon B8-10	88	1485	2.231	14.4	111	41	1144	35	2.25	0.44	5.7	1.9	22	517	0.11	1
Lithium exploratory well																
Cane Creek 32	335	6083	38.91	4.2	1058	1136	1098	473	20.54	1.01	8.9	14	1772	7185	0.48	0.08

*bdl: below detection limit
†na: not analyzed

TABLE 3. CALCULATED SATURATION INDICES AND DIC OF WATER SAMPLES USING PHREEQC

Sample/ Well ID	Barite	Calcite	Dolomite	Gypsum	Halite	Sylvite	CuS	Chalcocite	Chalcopyrite	DIC (meq/L)
Surface water and seeps										
DR-BR-a	0.4	-0.5	-1.4	-2.0	-6.6	-7.1	4.9	-8.0	13.3	2.87
DR-BR-b	0.8	0.6	0.9	-1.4	-5.9	-6.7	2.0	-14.4	10.0	3.47
DR North-a	0.4	-0.2	-0.4	-1.8	-4.7	-5.5	4.9	-8.5	13.8	2.97
DR-North-b	0.8	0.7	1.6	-1.1	-3.1	-4.0	1.5	-15.3	9.7	4.66
Salt Creek 1a	0.1	0.1	0.2	-0.5	-2.3	-3.3	3.6	-10.1	12.5	5.01
Salt Creek 1b	0.5	0.6	1.4	-0.5	-1.7	-2.7	2.0	-13.7	10.7	2.93
Salt Creek 2	0.6	-0.2	-0.5	-0.1	-4.1	-5.1	3.1	-11.2	12.6	6.93
Salt Creek Seep1	0.0	0.2	0.5	-0.6	-1.6	-2.5	3.8	-10.2	12.5	5.34
Salt Creek Seep2	0.5	0.8	1.6	-0.2	-3.6	-4.7	1.0	-15.6	9.6	5.58
Groundwater monitoring wells										
PW-3a	nd*	-0.2	-0.5	-0.6	-7.5	-7.8	nd	nd	nd	12.59
PW-3b	0.2	0.5	0.8	-0.6	-7.6	-7.8	nd	nd	nd	8.37
PW-4	0.0	0.0	-0.4	-0.3	-7.8	-8.1	nd	nd	nd	10.74
PW-12a	nd	0.1	0.1	-0.8	-7.2	-7.8	nd	nd	nd	8.33
PW-12b	0.1	0.3	0.5	-0.9	-7.1	-7.9	nd	nd	nd	7.47
325	nd	0.0	0.0	-2.0	-6.6	-7.5	nd	nd	nd	15.99
MW96-7A	nd	1.3	2.5	-0.5	-7.2	-7.7	nd	nd	nd	5.88
PW-7a	-0.2	0.3	0.4	-1.9	-7.0	-7.8	nd	nd	nd	4.40
PW-7b	nd	-0.6	-1.4	-1.9	-6.7	-7.4	nd	nd	nd	7.12
PW-8a	nd	-0.1	0.0	-2.1	-6.2	-7.1	nd	nd	nd	7.05
PW-8b	0.0	0.4	1.0	-2.1	-6.2	-7.1	nd	nd	nd	6.54
PW-11a	nd	0.3	0.6	-1.8	-6.4	-7.1	nd	nd	nd	4.36
PW-11b	-0.1	0.3	0.5	-1.9	-6.4	-7.2	nd	nd	nd	4.98
LV-41-75	nd	-0.5	-1.2	-2.4	-8.2	-8.6	nd	nd	nd	5.34
MW97-11	nd	0.7	1.3	-1.5	-6.4	-7.2	nd	nd	nd	6.58
MW97-13	nd	-0.5	-1.2	-1.8	-7.0	-7.6	nd	nd	nd	6.12
Brine pumping wells										
BOR well 2E	0.1	-0.2	0.1	0.0	-0.4	-1.4	2.6	-11.3	10.5	9.28
BOR well 3E	0.2	-0.3	0.0	0.0	-0.4	-1.5	2.4	-11.6	10.2	8.93
BOR well 8E	0.2	-0.8	-1.0	0.0	-0.5	-1.5	2.5	-11.6	10.4	7.84
BOR well 9E	0.3	-0.2	0.1	0.1	-0.5	-1.5	2.6	-11.4	10.7	7.48
Oil/gas producing wells										
MM 31-42	0.4	0.1	-0.5	-0.3	-1.9	-3.1	nd	nd	nd	1.43
MM 31-31	nd	1.0	1.3	-0.5	-1.1	-2.1	nd	nd	nd	42.57
MM 5-6	nd	1.5	2.5	-0.4	-0.3	-1.6	nd	nd	nd	18.90
HC 12-13	1.0	nd	nd	-0.5	-1.5	-2.5	3.3	-8.6	15.0	3.69
FF-5	1.8	nd	nd	-0.5	-1.2	-2.2	2.4	-10.8	13.8	3.79
Big Indian 24-31	1.6	nd	nd	-0.4	-1.1	-2.4	3.8	-8.0	14.8	13.71
BH 10-31	2.3	nd	nd	-0.6	-1.3	-2.5	1.1	-13.7	11.2	3.29
BH 10-42	1.8	nd	nd	-0.6	-1.2	-2.6	1.2	-13.2	11.7	8.72
Anasazi 1	0.1	-1.2	-2.7	-0.9	-2.4	-4.3	2.3	-10.8	10.9	2.16
Runway-10-E2	-0.1	nd	nd	-0.1	-0.7	-2.0	1.4	-13.4	11.1	2.70
Sahgzie 1a	-0.2	0.9	1.6	-0.1	-0.6	-1.9	1.8	-11.4	11.3	9.57
Sahgzie 1b	nd	1.2	2.2	-0.3	-0.5	-1.9	nd	nd	nd	9.18
Monument-8N-2a	0.1	0.7	1.1	0.0	-0.8	-2.0	0.4	-14.3	10.4	31.26
Monument-8N-2b	nd	1.0	1.7	0.0	-0.6	-1.8	nd	nd	nd	37.06
WM 22-43	-0.1	nd	nd	-0.2	-1.8	-3.2	0.1	-16.6	8.0	6.71
WM 34-24	-0.1	0.0	-0.2	-0.2	-2.0	-3.3	-0.4	-17.3	6.8	22.60
WM 34-31	-0.3	0.0	-0.2	-0.2	-2.0	-3.3	-0.3	-16.8	7.1	21.48
WM 34-33	-0.2	0.1	0.0	-0.2	-2.0	-3.3	-0.3	-17.1	7.0	21.53
Injection water	0.4	0.6	0.9	-0.2	-1.8	-3.2	nd	nd	nd	11.63
TOHO 35-B	0.1	nd	nd	-0.2	-0.7	-2.4	0.3	-16.1	10.3	2.78
TOHO 1	0.5	1.7	3.1	-0.4	-2.0	-3.5	nd	nd	nd	14.62
McIntyre 17-21	0.5	0.7	1.0	-0.3	-1.9	-2.7	0.9	-15.2	11.0	19.18
Lisbon 10-33	1.0	nd	nd	0.0	-0.7	-1.8	2.1	-10.3	12.6	15.46
Lisbon B8-10	0.3	1.2	2.0	-0.2	-1.7	-2.5	3.0	-11.1	13.4	14.84
Lithium exploratory well										
Cane Creek 32	-0.4	nd	nd	-0.1	-0.4	-0.7	2.3	-9.5	12.2	0

*nd: no data

Dissolved inorganic carbon (DIC) is equal to the sum of calculated HCO_3 and H_2CO_3

TABLE 4. ISOTOPIC DATA OF WATER SAMPLES COLLECTED IN THE STUDY AREA

Sample/Well ID	$\delta^{18}O_{water}$ ‰ (VSMOW)	δD_{water} ‰ (VSMOW)	$\delta^{34}S_{SO4}$ ‰ (CDT)	$\delta^{18}O_{SO4}$ ‰ (VSMOW)	$\delta^{34}S_{H2S}$ ‰ (CDT)	$^{87}Sr/^{86}Sr$
Surface water and seeps						
DR-BR-a	-12.30	-93.16	-0.99	4.12	na*	0.70966
DR-BR-b	-8.75	-73.02	-13.41	1.50	na	0.70912
DR North-a	-12.40	-94.00	5.75	7.26	na	0.70922
DR-North-b	-9.81	-79.28	6.23	7.41	na	0.70874
Salt Creek 1a	-13.65	-104.15	13.70	4.88	-10.7	0.70878
Salt Creek 1b	-12.29	-97.77	14.20	8.44	na	0.70874
Salt Creek 2	-14.71	-108.81	22.58	7.61	14.9	0.70877
Salt Creek Seep1	-14.01	-105.16	14.79	8.03	-19.8	0.70874
Salt Creek Seep2	-14.17	-106.07	15.95	9.91	na	0.70876
Groundwater monitoring wells						
PW-7a	-16.90	-127.21	na	na	na	0.70963
PW-7b	-17.00	-128.00	6.30	4.00	na	na
PW-8a	-17.00	-128.00	3.99	3.17	na	na
PW-8b	-12.23	-81.61	na	na	na	0.70920
PW-11a	-17.00	-128.00	8.88	5.71	na	na
PW-11b	-17.28	-129.35	na	na	na	0.70970
LV-41-75	-13.50	-102.00	4.29	-2.04	na	0.70960
MW97-11	-17.20	-129.00	3.80	4.00	na	0.70935
MW97-13	-17.40	-130.00	4.00	2.50	na	0.70958
MW06-15	-16.60	-126.00	na	na	na	na
PW-3a	-12.60	-95.00	-8.10	-5.80	na	na
PW-3b	-12.78	-95.21	na	na	na	0.70946
PW-4	-12.05	-89.04	na	na	na	0.70947
PW-12a	-14.80	-111.00	0.06	-2.32	na	na
PW-12b	-14.66	-109.51	na	na	na	0.70932
325	-15.90	-119.00	na	na	na	0.70926
MW96-7A	-12.90	-97.00	-1.73	-3.20	na	0.70936
98R7	-16.50	-124.00	na	na	na	na
98R4	-15.30	-114.00	na	na	na	na
PW-1	-15.60	-119.00	na	na	na	na
PW-2	-10.20	-82.00	na	na	na	na
Brine pumping wells						
BOR well 2E	-14.70	-110.18	14.17	9.11	-23.5	0.70868
BOR well 3E	-14.65	-110.86	14.27	8.98	-23.8	0.70863
BOR well 8E	-14.66	-110.84	14.47	11.93	-24.6	0.70867
BOR well 9E	-14.71	-110.48	14.29	8.46	-24.4	0.70868
Oil/gas producing wells						
MM 31-42	-4.48	-46.99	na	na	na	0.70954
MM 31-31	-5.23	-62.11	na	na	na	na
MM 5-6	1.61	-21.54	na	na	na	na
HC 12-13	-4.32	-48.70	6.90	10.45	na	0.70966
FF-5	-5.44	-53.48	-3.32	7.03	na	0.71204
Big Indian 24-31	-4.58	-48.10	na	na	na	0.70946
BH 10-31	-7.80	-74.88	9.64	12.66	na	0.70956
BH 10-42	-7.45	-73.57	14.51	14.10	na	0.70948
Anasazi 1	-10.12	-81.72	11.04	10.65	na	0.70930
Runway-10-E2	-1.50	-49.48	15.62	11.12	na	0.70866
Sahgzie 1a	4.32	-32.55	15.88	12.18	na	0.70851
Sahgzie 1b	4.93	-32.88	na	na	na	na
Monument-8N-2a	2.99	-37.33	17.57	13.04	na	0.70865
Monument-8N-2b	4.96	-34.57	na	na	na	na
WM 22-43	-6.58	-73.30	23.14	13.44	na	0.70859
WM 34-24	-7.90	-77.03	25.62	14.23	na	0.70855
WM 34-31	-7.92	-76.19	24.71	13.04	na	0.70861
WM 34-33	-8.51	-79.60	24.05	14.66	na	0.70852
Injection water	-6.48	-73.43	23.99	14.00	na	0.70856
TOHO 35-B	4.58	-32.04	18.73	16.46	na	0.70845
TOHO 1	-1.30	-66.05	33.62	9.82	na	0.70851
McIntyre 17-21	-8.20	-80.65	15.29	9.44	na	0.71753
Lisbon 10-33	0.91	-35.12	12.49	11.21	na	0.71281
Lisbon B8-10	4.36	-63.16	17.44	8.72	na	0.71375
Lithium exploratory well						
Cane Creek 32	4.98	-7.57	12.88	10.51	na	0.70843

*na: not analyzed